# Revisiting radiocarbon dating of lime mortar and lime plaster from Jerash in Jordan

Daugbjerg, Thomas Schrøder; Lichtenberger, Achim; Lindroos, Alf; Raja, Rubina; Olsen, Jesper

*Published in:*
Journal of archaeological science: Reports

*DOI:*
10.1016/j.jasrep.2021.103244

Published: 01/02/2022

*Document Version*
Final published version

*Document License*
CC BY

Journal of Archaeological Science: Reports 41 (2022) 103244

Contents lists available at ScienceDirect

Journal of Archaeological Science: Reports

journal homepage: www.elsevier.com/locate/jasrep

# Revisiting radiocarbon dating of lime mortar and lime plaster from Jerash in Jordan: Sample preparation by stepwise injection of diluted phosphoric acid

Thomas Schrøder Daugbjerg [a,b,*], Achim Lichtenberger [c], Alf Lindroos [d], Rubina Raja [b,e], Jesper Olsen [a,b]

[a] Aarhus AMS Centre (AARAMS), Department of Physics and Astronomy, Aarhus University, Aarhus, Denmark
[b] Centre for Urban Network Evolutions (UrbNet), Moesgård Allé 20, DK-8270 Højbjerg, Aarhus University, Denmark
[c] Institut für Klassische Archäologie und Christliche Archäologie/Archäologisches Museum, University of Münster, Germany
[d] Faculty of Science and Technology, Åbo Akademi University, Turku, Finland
[e] Department of History and Classical Studies, Institute for Culture and Society, Aarhus University, Denmark

ARTICLE INFO

*Keywords:*
Jerash
Mortar dating
Plaster dating
Radiocarbon dating
Stepwise injection
Cathodoluminescence

ABSTRACT

Ancient Gerasa (its Greco-Roman name)/Islamic Jerash (its later Arab name) is one of the most well-known pre-modern urban sites in northern Jordan, which flourished throughout antiquity and into the early Islamic period. Direct dating of mortar and plaster in Jerash is challenging due to the area's abundance of geological carbonates that hamper the use of radiocarbon mortar methodologies as shown by previous attempts. Therefore, this study revisited the important problem of Jerash mortar dating. The aim was to advance solutions to the challenges with geological carbonates through sample pre-treatment and preparation methods such as wet sieving, sedimentation, cryo2sonic and stepwise injection of diluted acid. To characterize the samples we used alkalinity screening and cathodoluminescence microscopy. Ten plaster samples from an Umayyad house, destroyed by the earthquake in 749 CE, in Jerash were radiocarbon dated. These produced 12 conclusive dates out of 20 attempted datings, and here some samples had multiple attempted datings. These dates confirmed the early Islamic date of the house structure, while some samples suggested reuse of older material. Five comparative mortar samples from medieval Finland and Sweden critically evaluated the methodology proposed in this article. These have known ages, and they produced five conclusive dates that compared accurately with the expected ages. Compared to previous attempts at Jerash mortar dating, this study made substantial contributions to Jerash mortar dating.

## 1. Introduction

Ancient Gerasa, later known as Jerash, is one of the famous urban sites in northwest Jordan belonging to the Roman Decapolis (Lichtenberger, 2003; Raja, 2012). The site has a long history, which stretches back into prehistoric times, but the main and monumental remains stem from the Roman periods onwards (e.g. Lichtenberger et al., 2018; 2019; 2020). Following a devastating earthquake in January 749 CE the city contracted immensely. From the early 20th century to the present, excavations have explored Jerash, where the abundant archaeological record enables studies of monuments, public buildings, domestic structures and everyday life in multiple cultural periods. Since 2011, the Danish-German Jerash Northwest Quarter Project has been undertaking archaeological research in an area of about 4 ha situated on the highest point within the city walls. This area has yielded extensive remains from the Roman period until the middle of the eight century CE, with an abrupt break in settlement until the Middle Islamic period (Lichtenberger and Raja, 2019). On the so-called Eastern Terrace, a set of Umayyad structures belonging to private houses have been excavated (trenches K, P and V in Fig. 1) (Barfod et al., 2015; Lichtenberger et al., 2016; Lichtenberger and Raja, 2017). These houses originate from the Umayyad period, without earlier forerunners, and the 749 CE earthquake destroyed them (Kalaitzoglou et al., forthcoming 1; Kalaitzoglou et al., forthcoming 2). Since the earthquake, human activity hardly

* Corresponding author at: Aarhus AMS Centre, Department of Physics and Astronomy, Aarhus University, Ny Munkegade 120, DK-8000 Aarhus C, Denmark.
*E-mail address:* thomas.daugbjerg@phys.au.dk (T.S. Daugbjerg).

https://doi.org/10.1016/j.jasrep.2021.103244
Received 14 April 2021; Received in revised form 27 September 2021; Accepted 25 October 2021
Available online 11 December 2021

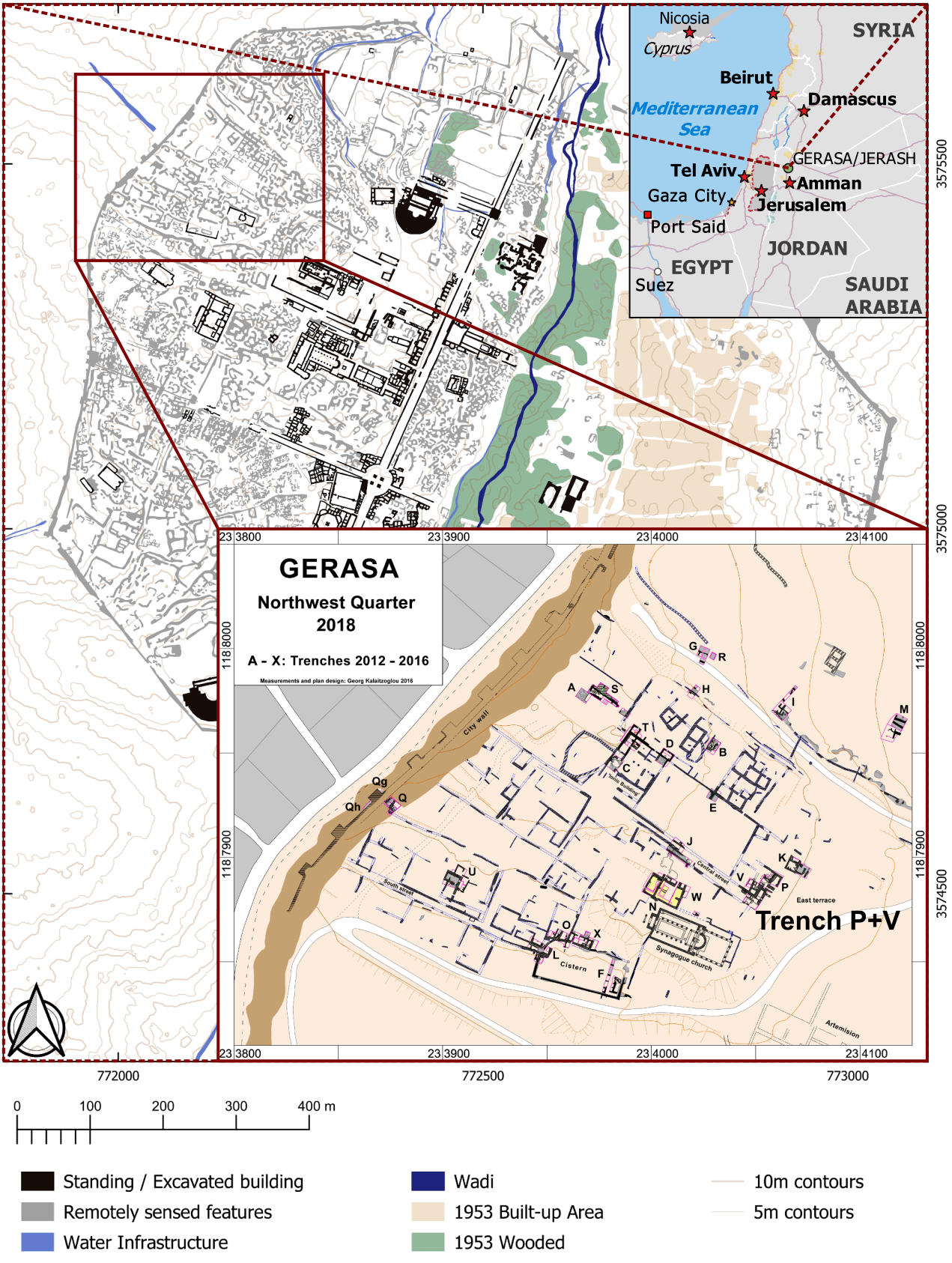


**Fig. 1.** Maps of the Northwest Quarter, ancient Jerash and the Middle East. (Maps credit: Danish-German Jerash Northwest Quarter Project).

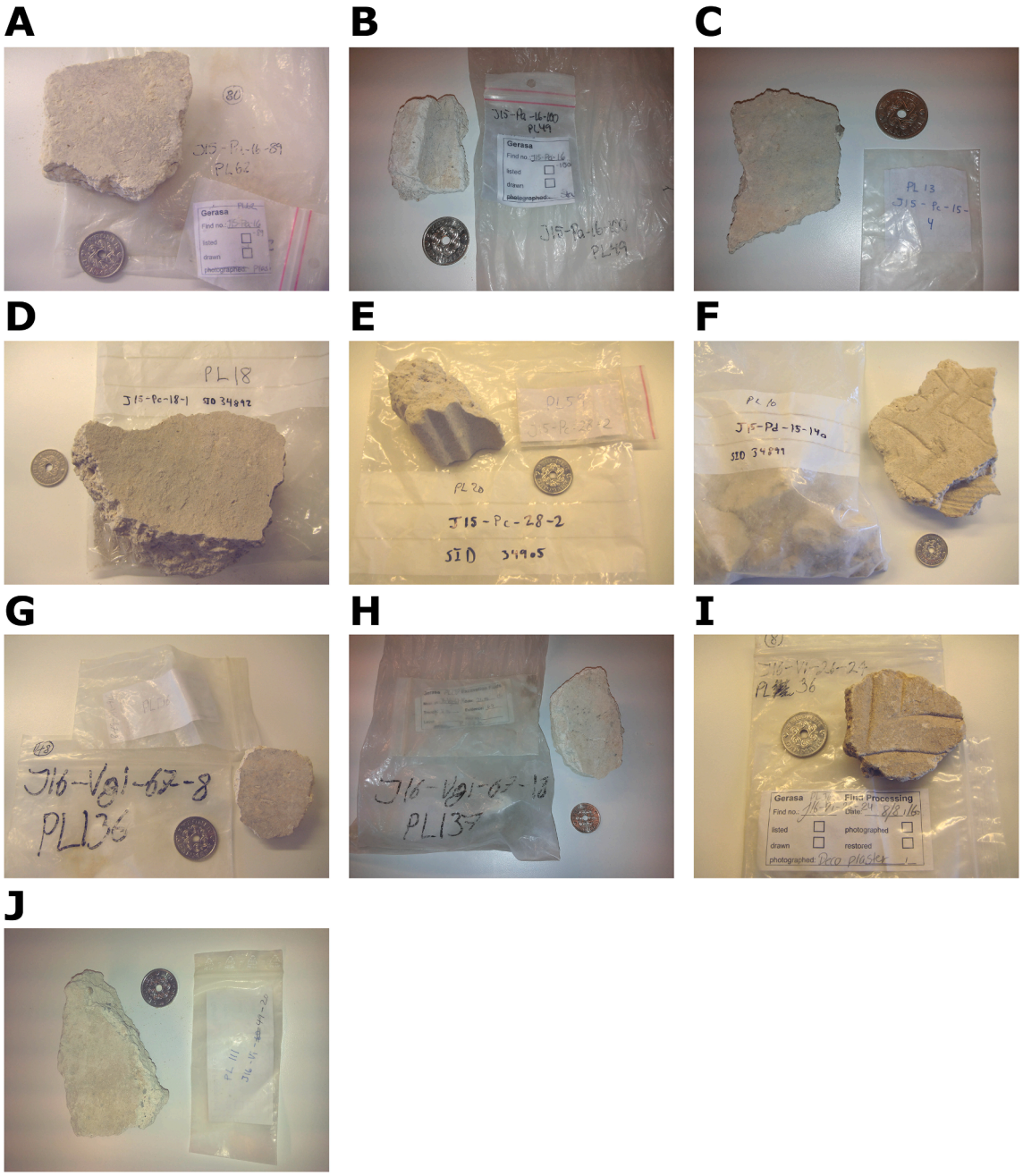


**Fig. 2.** Plaster samples from the Umayyad house. The coin has a diameter 28.5 mm. Thomsen (2019) discusses samples further. A J15-Pa-16-89, plaster. B J15-Pa-16-100, stucco. C J15-Pc-15-4, plaster. D J15-Pc-18-1, plaster from a ceramic water pipe. E J15-Pc-28-2, stucco. F J15-Pd-15-140, plaster with indentation pattern and embedded ceramic. G J16-Vgi-67-8, plaster. H J16-Vgi-67-18, plaster. I J16-Vi-26-24, plaster with indentation pattern. J J16-Vi-49-20, plaster.

disturbed the houses. Therefore, they present important case studies of domestic Umayyad finds, inventories and architecture from the region, and have a firm terminus ante quem (January 18th, 749 CE). In this article, we focused on material stemming from the house excavated in trenches P and V, which at the time of the earthquake was undergoing renovation and repairs involving the laying of new mosaics as well as preparatory work undertaken for new wall plastering (Lichtenberger and Raja, 2017).

Radiocarbon dating of lime mortar and lime plaster works by utilising the production- and hardening-process of lime (Labeyrie and Delibrias, 1964; Stuiver and Smith, 1965; Heinemeier et al., 2010; Ringbom et al., 2014). Lime production heats limestone to temperatures exceeding 900 °C where the main constituent, calcite ($CaCO_3$), thermally decomposes to quicklime (CaO). Mixing of quicklime and water produces slaked lime ($Ca(OH)_2$). The last production step mixes slaked lime and aggregate, typically sand, and the wet building material is ready for application as mortar or plaster in construction work. Mortar and plaster harden by a chemical reaction where the slaked lime absorbs $CO_2$ from the atmosphere and transforms back to calcite ($CaCO_3$). This calcite is the lime binder, and it captures the atmospheric $^{14}C$ signal at the time of hardening and thereby makes radiocarbon dating feasible. In this study, mortar dating refers to both mortar- and plaster-samples.

Radiocarbon dating of lime mortar is challenging because contaminants that are chemically similar to the dating material ($CaCO_3$) may interfere with the $^{14}C$ activity being measured (Labeyrie and Delibrias, 1964; Stuiver and Smith, 1965; Lindroos et al., 2007). For example

geological carbonate, nearly completely void of $^{14}C$, from grains of limestone in the sand used as aggregate, or limestone fragments surviving the lime burning. Secondary carbonates, from open system conditions or delayed hardening, are also risks in mortar dating (see Daugbjerg et al. (2021b) for further details).

Mortar radiocarbon dating preparation methods handle the risks of geological carbonate and secondary carbonates by extracting a series of $CO_2$ fractions, a radiocarbon profile, from a sample (Lindroos et al., 2007; Heinemeier et al., 2010). Each fraction is radiocarbon dated separately and conclusiveness criteria evaluate the radiocarbon profile for contaminants disturbing the binder's $^{14}C$ signal (Heinemeier et al., 2010; Ringbom et al., 2014; Lindroos et al., 2018). Here, a mortar date derives only for a conclusive radiocarbon profile. The discussion section's subsection on conclusiveness criteria presents this study's conclusiveness criteria.

Lichtenberger et al. (2015) presented a study of a Roman period cistern on the south slope of the Northwest Quarter with several phases of usage extending beyond the Roman period. The study furthered the overall understanding of the chronology of Roman and Byzantine water management in Jerash, by using radiocarbon dating of mortar from the cistern's walls and floors.

However, Lichtenberger et al. (2015) found that dating of mortar samples from Jerash is difficult due to complications with secondary carbonate and geological carbonate from aggregate. Lichtenberger et al. (2015) prepared their samples with sequential dissolution (see the materials and methods section), and their results had many radiocarbon profiles that conclusiveness criteria evaluated inconclusive. I.e. for many samples, it was not possible to determine a mortar date. Cretaceous limestone formations dominate the geology at Jerash and limestone grains are abundant in fluvial sediments of the local tributaries of the Zarqa River (Lichtenberger et al., 2015; Holdridge, 2020). Petrography of Jerash mortar reported sand, gravel and pebbles of local limestone in the mortar aggregate (Yaseen et al., 2013). One view of the results in Lichtenberger et al. (2015) is that contamination by fine grained geological carbonate from aggregate is the main challenge of mortar dating in Jerash.

The above-mentioned challenges of Jerash mortar dating motivated further research in mortar dating methodologies. This study aimed to bring together methodological advances, compared to the 2015 study, for Jerash mortar dating. The investigated methodologies were wet sieving, sedimentation, cryo2sonic and stepwise injection. Furthermore, known age samples from Dalby (Sweden), Turku (Finland) and Åland (Finland) were included to supplement the methodological investigation on removing geological carbonates.

## 2. Materials and methods

### 2.1. Plaster samples from the Umayyad house, Jerash

There were 10 unknown age plaster samples from the Umayyad house in trenches P and V (see Figs. 1, 2 and Table 1). The Umayyad house was excavated within the framework of the Danish-German Jerash Northwest Quarter Project, and the project collected the plaster samples in 2015 and 2016. Trenches P and V covered parts of the Umayyad house, and the trenches excavated buried rubble of the multistory building that was collapsed to ground floor level (Lichtenberger and Raja, 2017; Kalaitzoglou et al., forthcoming 1; Kalaitzoglou et al., forthcoming 2). Trench P identified main phases: bedrock, two Umayyad phases and the earthquake destruction event (Kalaitzoglou et al., forthcoming 1). The latest Umayyad phase in trench P was clearly associated with new clay floors (Lichtenberger and Raja, 2017). Trench V identified main phases: bedrock, a Byzantine phase, three Umayyad phases and the earthquake destruction event (Kalaitzoglou et al., forthcoming 2). This study's Jerash plaster samples were a mix from the Umayyad phases and the earthquake destruction event. The excavation picked loose plaster pieces in the trenches, since this had all fallen from the walls in the course of the sudden earthquake destruction (Lichtenberger and Raja, 2017).

All things considered, the samples' expected ages are Jerash's Umayyad era (640–749 CE (Thomsen, 2019)) or they could be older, if the Umayyad house reused building elements or rubble for filling (see the discussion). As such, the Jerash samples could not test new methodology, and therefore the next subsection presents known age samples with secure context and sample ages known a priori.

### 2.2. Known age mortar samples from Finland and Sweden

Table 1 lists 5 mortar samples with known ages and secure contexts to buildings from medieval Finland and Sweden. The samples had varying contents of geological carbonate, and this study quoted existing or published radiocarbon profiles by sequential dissolution for the known age samples (see the respective references for further details). These samples tested and evaluated the proposed mortar dating methodologies' feasibility, and provided a comparison between sequential dissolution and stepwise injection.

Samples Dalby001 and Dalby009 are from the northern wall of Dalby church in Scania, Sweden (Lindroos et al., 2014). King Sven Estridsson (reigning 1047–1076 CE) erected the church, and we compared with IntCal20's $^{14}C$ minimum during his reign, $914 \pm 10$ $^{14}C$ years BP in 1056 CE (Reimer et al., 2020).

Sample Fika057 is from the nave of Finström church on the Åland Islands, Finland. Heinemeier et al. (2010) presented mortar dating results that agreed with wood sample Fika061W, radiocarbon dated to $391 \pm 33$ $^{14}C$ years BP.

Sample Saka110 is from the tower of Saltvik church on the Åland Islands, Finland. Heinemeier et al. (2010) presented mortar dating results that agreed with wood sample Saka163W radiocarbon dated to $615 \pm 35$ $^{14}C$ years BP.

Sample TTK006 is from the pentagonal choir of Turku cathedral, Finland (Lindroos et al., 2011a). The choir was built soon after the inauguration of the cathedral in 1300 CE (Gardberg et al., 2000). We considered 1300 CE, with a radiocarbon value of $659 \pm 11$ $^{14}C$ years BP (Reimer et al., 2020), accurate for the time of construction. Sample TTK006 could also belong to reparations following a Novgorodian raid in 1318 CE (Gardberg et al., 2000).

### 2.3. Sample pre-treatment

As seen in Fig. 2, the plaster- and stucco-samples had a smooth and easily identifiable surface. The surface-near part of a sample, e.g. the material from this smooth surface to a depth of a few centimetres, likely hardened with good atmospheric contact, and the surface-near material is the better option when minimizing the risk of delayed hardening (Daugbjerg et al., 2021b). This considered, hammer and chisel separated surface-near material from a sample, and the following pre-treatment methods used this material. The surface-near material separated from a sample was typically pieces with thicknesses 1.0–3.5 cm and combined mass 10–50 g. A coarse brush and a soft brush cleaned the separated near-surface material.

#### 2.3.1. Cryogenic breaking

The samples were cryogenically broken, as described by Nawrocka et al. (2005) and Marzaioli et al. (2013). A sample underwent freeze–thaw cycles, in liquid nitrogen and an 80 °C oven. Pliers then crushed

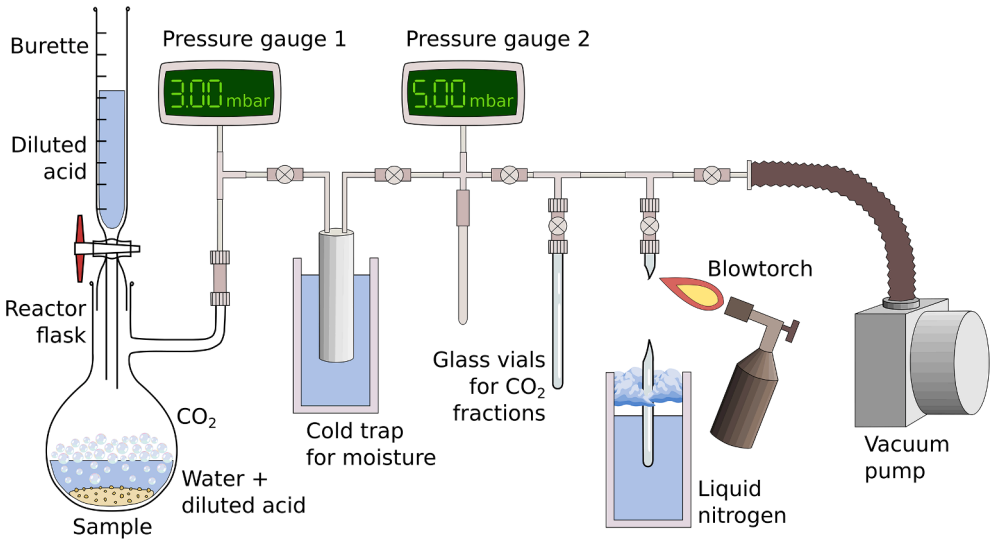


**Fig. 3.** The experimental setup for stepwise injection. Figure inspired by Ringbom et al. (2014).

the sample (Heinemeier et al., 2010).

### 2.3.2. *Wet sieving*

The crushed sample was dry sieved by hand to obtain several grain size fractions using meshes 100–500 μm (Van Strydonck et al., 1986; Van Strydonck et al., 1992). The grain size fractions < 125 μm were wet sieved using ultra-pure water (EMD Millipore 2013) to obtain several grain size fractions. Centrifuging at 3500 rpm (2300 G) for 5 min and a pipette removed the water, and the sample dried in an 80 °C oven.

### 2.3.3. *Sedimentation*

The < 38 μm grain size fraction, produced by wet sieving, was suspended in a 250 mL Labsolute screw cap bottle with ultra-pure water. Thorough shaking homogenised the suspension before sedimentation started. Stokes equation for sedimentation pre-calculated the sedimentation time based on the sedimentation height and desired grain size (Jackson and Saeger 1935; Ortega et al., 2012). A clock determined when time was up, and a pipette extracted the top water filling the sedimentation height. Sedimentation produced grain size fractions < 10 μm and < 4 μm.

### 2.3.4. *Cryo2sonic*

The cryo2sonic protocol pre-treated samples as described by Marzaioli et al. (2013), Nonni et al. (2013) and Barrett et al. (2020). Here an ultrasonic bath produced small particles from a cryogenically broken sample suspended in ultrapure water. See the references above for details. The name susp denoted this grain fraction.

## 2.4. *Characterization methods*

Alkaline mortar and plaster can absorb $CO_2$ after the hardening event, and they are thereby prone to have secondary carbonates (Heinemeier et al., 2010; Lichtenberger et al., 2015; Lindroos et al., 2007, 2011b). Therefore, alkalinity was characterized by suspending approximately 200 mg of the 125–250 μm grain size fraction in 10 mL deionized water and a pH electrode measured pH (Lindroos et al., 2011b; WTW, 2017). The reported pH value was the mean and standard deviation of measurements taken from 15 to 60 min in water, every 5th minute. The pH electrode similarly measured pH for three batches of approximately 200 mg crushed pure calcite crystals, and they served as stable calcite alkalinity-references. A sample was ruled significantly alkaline, if it failed a chi-square test for goodness of fit (Bennett and Franklin, 1954; Press et al., 1992) for the weighted mean of the pH values of the sample and the three alkalinity-references for stable calcite. I.e., it failed when the $\chi^2$-test-value (denoted T in the column with 'Alkalinity (pH)' in Table 1) exceeded the critical value $\chi^2(df = 3,\alpha = 5\%) = 7.8$. Here the critical value had degrees of freedom, df = 3, and significance level $\alpha = 5\%$.

The grain fractions produced by the pre-treatment methods, described in the subsection on sample pre-treatment in the materials and methods section, had subsamples taken and characterized with cathodoluminescence microscopy. Subsamples from the same grain fractions were prepared with sequential dissolution and/or stepwise injection and radiocarbon dated by AMS, see the materials and methods section. Cathodoluminescence characterization used a Dino Lite digital microscope combined with a Cambridge Image Technology Ltd (CITL) CL8200 MK4 cold cathode cathodoluminescence (CL) device (Marshall, 1988; Götze, 2012; Toffolo et al., 2020). In short, the CL system placed the sample in a vacuum where a beam of electrons excited the sample's luminescent minerals. Luminescent grains of the sample then lit up with mineral-specific colours, and this enabled mineral and mineral-phase identification. Abundant orange-red luminescent grains are a marker for geological carbonate.

## 2.5. *Sequential dissolution*

Sequential dissolution (SD) injected a single batch of excessive 85% $H_3PO_4$ on pre-treated sample powder under vacuum (Lindroos et al., 2007; Heinemeier et al., 2010; Ringbom et al., 2014). The acid dissolves binder carbonate and contaminating carbonate with different reaction rates. Secondary carbonates have the fastest rates, binder carbonate has a continuum from fast to slow rates and geological carbonate has the slowest rates. The setup collected a series of $CO_2$ fractions throughout the dissolution for subsequent $^{14}C$ analysis to differentiate the $CO_2$ origins. This study did not undertake new sequential dissolution, but quoted published sequential dissolution results from Lindroos et al.

(2011a) and Heinemeier et al. (2010), and unpublished sequential dissolution results from Lindroos et al. (2014).

### 2.6. Stepwise injection

Considering the work of Al-Bashaireh (2013, 2015); Al-Bashaireh and Hodgins (2012); Hodgins et al. (2011); Van Strydonck et al. (1986, 1989, 1992), the order of different carbonate phases' reaction rates is the same in stepwise injection (SI) as in sequential dissolution. Fig. 3 illustrates the stepwise injection setup from this study. Ultra-pure water suspended the pre-treated sample powder in a reactor flask. A vacuum pump provided vacuum to the whole system. A burette injected batches of approximately 2.0 mL $3.0{\cdot}10^{-2}$ mol/L $H_3PO_4$ to produce a $CO_2$ fraction with approximately 0.4 mg carbon. Pressure gauge 1 measured the produced $CO_2$ increasing the pressure in the reactor flask. When the acid was depleted the reaction stopped, and one extracted a $CO_2$ fraction using liquid nitrogen. The system was then ready to repeat the process.

The cold trap removed moisture in the part of the vacuum system away from the reactor flask. Pressure gauge 2 had a calibrated volume and measured the size of produced fractions. Liquid nitrogen and a blowtorch sealed the fraction in a glass vial.

Prior to stepwise injection, 85% $H_3PO_4$ totally dissolved a small sample aliquot (approximately 10–20 mg), and the sample's total carbon yield was determined. Using the carbon yield, stepwise injection scaled the sample's mass, so five fractions covered the first 10% of the sample's carbon content (Table 1). Thereby it was possible to focus on the most rapidly dissolving material that is crucial for dating (Folk and Valastro, 1976). In sequential dissolution, this material dissolves so rapidly that it may be difficult to get more than one $CO_2$ fraction from the first 10% of the carbon inventory. In addition, because the sample powder was suspended in water and a diluted acid was used, instead of viscous 85% $H_3PO_4$, it was possible to dissolve more fine-grained sample powders than when using sequential dissolution.

### 2.7. Radiocarbon dating and statistical methods

Graphitization reactors produced graphite from the $CO_2$ fractions using hydrogen and an iron catalyst (Vogel et al., 1984). A pneumatic press pressed the graphite into AMS cathodes, and Aarhus AMS centre's HVE 1 MV accelerator radiocarbon dated the fractions (Olsen et al., 2017). Radiocarbon dates are reported as uncalibrated $^{14}C$ ages BP normalized to $\delta^{13}C = -25$ ‰ according to international convention using $^{13}C/^{12}C$ ratios measured by the AMS system (Stuiver and Polach, 1977). Graphite samples with mass lower than 0.7 mgC were blank corrected according to Donahue et al. (1990) and Brown and Southon (1997) (see also Daugbjerg et al. (2021a)). The online program OxCal 4.4 with the IntCal20 calibration curve converted radiocarbon ages to calendar ages (Bronk Ramsey, 2009; Reimer et al., 2020).

The conclusiveness criteria for $^{14}C$ profiles for stepwise injection were similar to criteria for sequential dissolution (Heinemeier et al., 2010). A chi-square test for goodness of fit evaluated if fractions' $^{14}C$ ages agreed (Bennett and Franklin, 1954; Press et al., 1992). If a stepwise injection result fulfilled one or more of the criteria, it was conclusive (Heinemeier et al., 2010). The conclusive sample age then derived from all fractions passing the criterion, and the discussion elaborates further on the used conclusiveness criteria.

## 3. Results

Table 1 presents results from characterization and radiocarbon dating for all samples, and the results section explains further.

### 3.1. Sample characterization

CL microscopy of various grain fractions was used to indicate possible contaminants. Here bright orange-red indicates limestone, and quartz and feldspar are indicated by blue and green colours, respectively (Lindroos et al., 2007; Al-Bashaireh, 2013). Fig. 4 and Table 1 summarise the CL results. Typically the smaller grain size exhibited the few to none bright orange-red colours, and hence the small grain size had low concentrations of geological carbonates (Fig. 4).

The samples J15-Pa-16-89, J15-Pc-15-4, J16-Vgi-67-8, Dalby001, Dalby009, TTK006 and Fika057 had a medium content of orange-red-grains in some of their radiocarbon dated grain fractions. For these, one had to consider geological carbonate (Table 1). Samples J15-Pd-15-140, J16-Vgi-67-18 and J16-Vi-26-24 were significantly more alkaline than the calcite references (Table 1), and one had to consider the risk of secondary carbonates, as explained in materials and methods.

### 3.2. Radiocarbon profiles from the known age samples

Fig. 5 shows radiocarbon profiles by sequential dissolution and stepwise injection for the known age samples Dalby001, Dalby009, Fika057, Saka110 and TTK006. The calculation of Z scores used the known ages from Table 2. Table 1 presents known age samples' fractions in $^{14}C$ years. Notice the different scale of abscissae between sequential dissolution and stepwise injection. The former extracted approximately 0.5 to 1.0 of a sample's carbon inventory, while the latter extracted approximately 0.1 of a sample's carbon inventory (as targeted). See the materials and methods section for further details on the operation of the preparation methods. Due to a combination of quoted and new radiocarbon profiles, Fig. 5 have differences between the grain size fractions of sequential dissolution and stepwise injection.

For samples Dalby001, Dalby009, Saka110 and TTK006 there were sequential dissolution profiles where later fractions had increasingly higher Z scores, i.e. older $^{14}C$ ages. Some of the last fractions were above the + 2 Z score boundary, i.e. fractions too old. The stepwise injection profiles in Fig. 5 largely had fractions inside the ± 2 Z score region, albeit Dalby001 and Saka110 had early fractions below the −2 Z score boundary, i.e. fractions too young. In addition, TTK006 had some fractions above the + 2 Z score boundary, i.e. fractions too old.

### 3.3. Radiocarbon profiles from the Umayyad house in trenches P and V

Fig. 6 shows examples of radiocarbon profiles for samples from the Umayyad house in trenches P and V. The profiles J15-Pc-15-4, <38 μm and 15-Pc-15-4, <10 μm in Fig. 6A and J15-Pc-18-1, 38-63 μm in Fig. 6B had homogenous $^{14}C$ profiles. The weighted average of all fractions in the J15-Pc-15-4, <38 μm profile passed a chi-square test df = 4 T = 6.5 (5% 9.5), and the mean and standard deviation was 1358 ± 35 $^{14}C$ years BP. The weighted average of all fractions in the J15-Pc-18-1, 38–63 μm profile passed a chi-square test df = 4 T = 6.5(5% 9.5), and the mean and standard deviation was 1646 ± 31 $^{14}C$ years BP.

The profiles J15-Pc-15-4, 38–63 μm in Fig. 6A, J15-Pc-28-2, <4 μm in Fig. 6C and J16-Vgi-67-8, <10 μm in Fig. 6E had later fractions increasingly older, while the first two fractions' $^{14}C$ ages agreed. In Fig. 6C the weighted average of the first two fractions of J15-Pc-28-2, <4 μm was 1362 ± 21 $^{14}C$ years BP and passed a chi-square test with df = 1 T = 0.0(5% 3.8). In Fig. 6E the weighted average of the first two fractions of J16-Vgi-67-8, <10 μm was 1777 ± 24 $^{14}C$ years BP and passed a chi-square test with df = 1 T = 0.7(5% 3.8).

Other profiles in Fig. 6 covered a wide range of $^{14}C$ ages and their earliest fractions did not agree in $^{14}C$ age. Table 1 lists further radiocarbon profiles from the Umayyad house.

**Table 1**
Mortar and plaster samples by preparation method, with characterization results and radiocarbon dated $CO_2$ fractions. Sequential dissolution profiles for Dalby001 and Dalby009 were made by Lindroos et al. (2014) but unpublished. Sequential dissolution profiles for Fika057, Saka110 and TTK006 quoted from Heinemeier et al. (2010) and Lindroos et al. (2011a). For the quoted sequential dissolution radiocarbon profiles, the mass of sample and fractions was not available. The quoted radiocarbon profiles had $\delta^{13}C_{AMS}$ measured by splitting an aliquot and using a GV Instruments Isoprime stable isotope mass spectrometer, and such $\delta^{13}C_{AMS}$ values are marked with an asterisk. Grain fractions marked with two asterisks were pre-treated without cryogenic breaking. CL of Fika057 quoted from Heinemeier et al. (2010) and CL of TTK006 quoted from (Daugbjerg et al., 2021a). The stable calcite references for alkalinity had pH values 9.65 ± 0.05, 9.62 ± 0.04 and 9.58 ± 0.03.

| Sample<br>Material<br>Preparation method | Grain fraction<br>Carbon yield (%)<br>Mass (mg) | CL orange-red grains<br>Alkalinity (pH)<br>$\chi^2$ test alkalinity | Laboratory no. | Reaction time (s) | Cumulative $CO_2$ fraction | Fraction mass (mgC) | $^{14}$C age ($^{14}$C years BP) | $\delta 13C_{AMS}$ (‰ VPDB) | Conclusiveness criteria | Conclusive age ($^{14}$C years BP)<br>χ2-test |
|---|---|---|---|---|---|---|---|---|---|---|
| J15-Pa-16–89 | 38–63 μm | Medium | AAR-32813.SI1.1 | 900 | 0–0.0125 | 0.26 | 1416 ± 30 | –22 | CIII + CIV | 1382 ± 35 |
| Plaster | 10% | 9.60 ± 0.06 | AAR-32813.SI1.2 | 1680 | 0.0125–0.0277 | 0.31 | 1650 ± 28 | −15 | (J15-Pa-16–100, susp) | (mean ± std) |
| Stepwise injection | 197.9 mg | df=3 T=0.0(5% 7.8) | AAR-32813.SI1.3 | 2640 | 0.0277–0.0412 | 0.28 | 1830 ± 35 | −15 | | df=1 T=2.6(5% 3.8) |
| | | | AAR-32813.SI1.4 | 3450 | 0.0412–0.0653 | 0.49 | 1799 ± 28 | −15 | | |
| | | | AAR-32813.SI1.5 | 4260 | 0.0653–0.0895 | 0.49 | 1750 ± 28 | −18 | | |
| J15-Pa-16–89 | <38 μm | Few | AAR-32813.SI2.1 | 480 | 0–0.0173 | 0.35 | 1656 ± 29 | −15 | | – |
| Plaster | 13% | 9.60 ± 0.06 | AAR-32813.SI2.2 | 1140 | 0.0173–0.0345 | 0.35 | 1803 ± 38 | −12 | | – |
| Stepwise injection | 158.9 mg | df=3 T=0.0(5% 7.8) | AAR-32813.SI2.3 | 1830 | 0.0345–0.0518 | 0.35 | 2040 ± 30 | −12 | | |
| | | | AAR-32813.SI2.4 | 2640 | 0.0518–0.0681 | 0.33 | 2284 ± 32 | −13 | | |
| | | | AAR-32813.SI2.5 | 3540 | 0.0681–0.0865 | 0.37 | 2318 ± 31 | −12 | | |
| J15-Pa-16–89 | <10 μm | Few | AAR-32813.SI3.1 | 480 | 0–0.0149 | 0.29 | Lost | Lost | | – |
| Plaster | 8.5% | 9.60 ± 0.06 | AAR-32813.SI3.2 | 1170 | 0.0149–0.0325 | 0.35 | 1847 ± 33 | −13 | | – |
| Stepwise injection | 231.3 mg | df=3 T=0.0(5% 7.8) | AAR-32813.SI3.3 | 2040 | 0.0325–0.0502 | 0.35 | 1832 ± 32 | −12 | | |
| | | | AAR-32813.SI3.4 | 2880 | 0.0502–0.0669 | 0.33 | 2030 ± 32 | −13 | | |
| | | | AAR-32813.SI3.5 | 3720 | 0.0669–0.0865 | 0.39 | 2309 ± 59 | −11 | | |
| J15-Pa-16–89 | <4 μm | Few | AAR-32813.SI4.1 | 540 | 0–0.0145 | 0.29 | 1602 ± 36 | −16 | | – |
| Plaster | 13% | 9.60 ± 0.06 | AAR-32813.SI4.2 | 1200 | 0.0145–0.0326 | 0.37 | 1807 ± 35 | −9 | | – |
| Stepwise injection | 155.1 mg | df=3 T=0.0(5% 7.8) | AAR-32813.SI4.3 | 1860 | 0.0326–0.0506 | 0.36 | 1849 ± 32 | −11 | | |
| | | | AAR-32813.SI4.4 | 2640 | 0.0506–0.0694 | 0.38 | 1833 ± 39 | −13 | | |
| | | | AAR-32813.SI4.5 | 3570 | 0.0694–0.0909 | 0.44 | 1933 ± 30 | −11 | | |
| J15-Pa-16–100 | <4 μm | None | AAR-32814.SI1.1 | 1500 | 0–0.0166 | 0.35 | 1170 ± 33 | −17 | CI | 1162 ± 23 |
| Plaster | 14% | 9.52 ± 0.08 | AAR-32814.SI1.2 | 2700 | 0.0166–0.0351 | 0.39 | 1155 ± 32 | −12 | CI | (weighted average) |
| Stepwise injection | 150.1 mg | df=3 T=4.5(5% 7.8) | AAR-32814.SI1.3 | 3540 | 0.0351–0.0527 | 0.37 | 1303 ± 32 | −12 | | df=1 T=0.1(5% 3.8) |
| | | | AAR-32814.SI1.4 | 4380 | 0.0527–0.0755 | 0.48 | 1403 ± 32 | −12 | | |
| | | | AAR-32814.SI1.5 | 5520 | 0.0755–0.0966 | 0.44 | 1417 ± 30 | −13 | | |
| J15-Pa-16–100 | susp | None | AAR-32814.SI2.1 | 450 | 0–0.0134 | 0.28 | 1347 ± 31 | −17 | CI | 1373 ± 26 |
| Plaster | 13% | 9.52 ± 0.08 | AAR-32814.SI2.2 | 1080 | 0.0134–0.0269 | 0.28 | 1399 ± 33 | −15 | CI | (mean ± std) |
| Stepwise injection | 163.0 mg | df=3 T=4.5(5% 7.8) | AAR-32814.SI2.3 | 1770 | 0.0269–0.0403 | 0.28 | 1467 ± 31 | −13 | | df=1 T=1.3(5% 3.8) |
| | | | AAR-32814.SI2.4 | 2460 | 0.0403–0.0526 | 0.25 | 1438 ± 35 | −15 | | |
| J15-Pc-15–4 | 38–63 μm | Medium | AAR-32815.SI1.1 | 1800 | 0–0.0200 | 0.40 | 1348 ± 27 | −16 | CI | 1367 ± 19 |
| Plaster | 7.6% | 9.68 ± 0.03 | AAR-32815.SI1.2 | 3420 | 0.0200–0.0427 | 0.46 | 1385 ± 27 | −13 | CI | (weighted average) |

(*continued on next page*)

**Table 1** (*continued*)

| Sample<br>Material<br>Preparation method | Grain fraction<br>Carbon yield (%)<br>Mass (mg) | CL orange-red grains<br>Alkalinity (pH)<br>$\chi^2$ test alkalinity | Laboratory no. | Reaction time (s) | Cumulative $CO_2$ fraction | Fraction mass (mgC) | $^{14}C$ age ($^{14}C$ years BP) | $\delta 13C_{AMS}$ (‰ VPDB) | Conclusiveness criteria | Conclusive age ($^{14}C$ years BP)<br>$\chi$2-test |
|---|---|---|---|---|---|---|---|---|---|---|
| Stepwise injection | 265.8 mg | df=3 T=2.9(5% 7.8) | AAR-32815.SI1.3 | 4560 | 0.0427–0.0590 | 0.33 | 1519 ± 31 | −17 | | df=1 T=0.9(5% 3.8) |
| | | | AAR-32815.SI1.4 | 5910 | 0.0590–0.0753 | 0.33 | 1462 ± 34 | −17 | | |
| | | | AAR-32815.SI1.5 | 6870 | 0.0753–0.0963 | 0.42 | 1512 ± 28 | −16 | | |
| J15-Pc-15–4 | <38 μm | Few | AAR-32815.SI2.1 | 1320 | 0–0.0174 | 0.35 | 1289 ± 31 | −15 | CI | 1358 ± 35 |
| Plaster | 11% | 9.68 ± 0.03 | AAR-32815.SI2.2 | 2100 | 0.0174–0.0321 | 0.29 | 1367 ± 32 | −13 | CI | (mean ± std) |
| Stepwise injection | 176.2 mg | df=3 T=2.9(5% 7.8) | AAR-32815.SI2.3 | 2820 | 0.0321–0.0496 | 0.35 | 1371 ± 30 | −13 | CI | df=4 T=6.5(5% 9.5) |
| | | | AAR-32815.SI2.4 | 3780 | 0.0496–0.0688 | 0.38 | 1381 ± 28 | −13 | CI | |
| | | | AAR-32815.SI2.5 | 4560 | 0.0688–0.0927 | 0.48 | 1380 ± 28 | −12 | CI | |
| J15-Pc-15–4 | <10 μm | None | AAR-32815.SI3.1 | 480 | 0–0.0147 | 0.29 | 1415 ± 36 | −15 | CI | 1399 ± 34 |
| Plaster | 9.2% | 9.68 ± 0.03 | AAR-32815.SI3.2 | 1260 | 0.0147–0.0361 | 0.42 | 1331 ± 31 | −13 | CI | (mean ± std) |
| Stepwise injection | 215.6 mg | df=3 T=2.9(5% 7.8) | AAR-32815.SI3.3 | 2040 | 0.0361–0.0517 | 0.31 | 1417 ± 42 | −12 | CI | df=4 T=5.8(5% 9.5) |
| | | | AAR-32815.SI3.4 | 2880 | 0.0517–0.0692 | 0.35 | 1420 ± 29 | −13 | CI | |
| | | | AAR-32815.SI3.5 | 3840 | 0.0692–0.0877 | 0.37 | 1410 ± 31 | −13 | CI | |
| J15-Pc-18–1 | 38–63 μm | Few | AAR-32812.SI1.1 | 1980 | 0–0.0275 | 0.31 | 1653 ± 32 | −13 | CI | 1646 ± 31 |
| Plaster | 5.7% | 9.47 ± 0.06 | AAR-32812.SI1.2 | 3210 | 0.0275–0.0565 | 0.33 | 1602 ± 28 | −14 | CI | (mean ± std) |
| Stepwise injection | 200.0 mg | df=3 T=3.9(5% 7.8) | AAR-32812.SI1.3 | 4080 | 0.0565–0.0905 | 0.38 | 1630 ± 32 | −15 | CI | df=4 T=6.5(5% 9.5) |
| | | | AAR-32812.SI1.4 | 4950 | 0.0905–0.123 | 0.37 | 1649 ± 28 | −15 | CI | |
| | | | AAR-32812.SI1.5 | 5940 | 0.123–0.164 | 0.46 | 1698 ± 27 | −14 | CI | |
| J15-Pc-28–2 | <4 μm | Few | AAR-32816.SI1.1 | 450 | 0–0.0164 | 0.33 | 1361 ± 29 | −14 | CI | 1362 ± 21 |
| Plaster | 13% | 9.70 ± 0.01 | AAR-32816.SI1.2 | 1110 | 0.0164–0.0355 | 0.39 | 1363 ± 30 | −9 | CI | (weighted average) |
| Stepwise injection | 158.8 mg | df=3 T=2.6(5% 7.8) | AAR-32816.SI1.3 | 2040 | 0.0355–0.0531 | 0.35 | 1481 ± 34 | −10 | | df=1 T=0.0(5% 3.8) |
| | | | AAR-32816.SI1.4 | 2730 | 0.0531–0.0686 | 0.31 | 1552 ± 33 | −10 | | |
| | | | AAR-32816.SI1.5 | 3540 | 0.0686–0.0923 | 0.48 | 1676 ± 28 | −8 | | |
| J15-Pd-15–140 | <4 μm | None | AAR-32817.SI1.1 | 540 | 0–0.0142 | 0.29 | 2015 ± 35 | −19 | | – |
| Plaster | 12% | 9.83 ± 0.01 | AAR-32817.SI1.2 | 1200 | 0.0142–0.0313 | 0.35 | 2328 ± 63 | −12 | | – |
| Stepwise injection | 167.8 mg | df=3 T=12(5% 7.8) | AAR-32817.SI1.3 | 1860 | 0.0313–0.0485 | 0.35 | 2572 ± 35 | −11 | | |
| | | | AAR-32817.SI1.4 | 2580 | 0.0485–0.0667 | 0.37 | 3223 ± 34 | −11 | | |
| | | | AAR-32817.SI1.5 | 3420 | 0.0667–0.0866 | 0.40 | 3062 ± 34 | −11 | | |
| J15-Pd-15–140 | susp | Medium | AAR-32817.SI2.1 | 390 | 0–0.0146 | 0.29 | 2121 ± 34 | −18 | | – |
| Plaster | 10% | 9.83 ± 0.01 | AAR-32817.SI2.2 | 1020 | 0.0146–0.0309 | 0.33 | 2517 ± 35 | −13 | | – |
| Stepwise injection | 198.3 mg | df=3 T=12(5% 7.8) | AAR-32817.SI2.3 | 1680 | 0.0309–0.0486 | 0.36 | 3063 ± 34 | −12 | | |
| | | | AAR-32817.SI2.4 | 2460 | 0.0486–0.0731 | 0.49 | 4095 ± 34 | −9 | | |
| J16-Vgi-67–8 | 38–63 μm | Medium | AAR-32818.SI1.1 | 1200 | 0–0.0186 | 0.37 | 1519 ± 27 | −18 | | – |
| Plaster | 10% | 9.5 ± 0.1 | AAR-32818.SI1.2 | 2580 | 0.0186–0.0421 | 0.46 | 2117 ± 26 | −14 | | – |
| Stepwise injection | 193.6 mg | df=3 T=1.1(5% 7.8) | AAR-32818.SI1.3 | 3420 | 0.0421–0.0654 | 0.46 | 2056 ± 29 | −17 | | |
| | | | AAR-32818.SI1.4 | 4380 | 0.0654–0.0886 | 0.46 | 2064 ± 27 | −17 | | |
| | | | AAR-32818.SI1.5 | 5220 | 0.0886–0.111 | 0.44 | 2141 ± 26 | −16 | | |
| J16-Vgi-67–8 | <38 μm | Few | AAR-32818.SI2.1 | 360 | 0–0.0173 | 0.35 | 1752 ± 31 | –22 | CIII | 1751 ± 23 |
| Plaster | 11% | 9.5 ± 0.1 | AAR-32818.SI2.2 | 1080 | 0.0173–0.0365 | 0.38 | 2179 ± 34 | −17 | | |

(*continued on next page*)

**Table 1** (*continued*)

| Sample<br>Material<br>Preparation method | Grain fraction<br>Carbon yield (%)<br>Mass (mg) | CL orange-red grains<br>Alkalinity (pH)<br>$\chi^2$ test alkalinity | Laboratory no. | Reaction time (s) | Cumulative $CO_2$ fraction | Fraction mass (mgC) | $^{14}C$ age ($^{14}C$ years BP) | $\delta 13C_{AMS}$ (‰ VPDB) | Conclusiveness criteria | Conclusive age ($^{14}C$ years BP)<br>$\chi$2-test |
|---|---|---|---|---|---|---|---|---|---|---|
| | | | | | | | | | (J16-Vgi-67–18, <4 μm) | (weighted average) |
| Stepwise injection | 187.8 mg | df=3 T=1.1(5% 7.8) | AAR-32818.SI2.3 | 1860 | 0.0365–0.0512 | 0.29 | 2169 ± 39 | −21 | | df=1 T=0.0(5% 3.8) |
| | | | AAR-32818.SI2.4 | 2640 | 0.0512–0.0694 | 0.37 | 2667 ± 34 | −17 | | |
| | | | AAR-32818.SI2.5 | 3660 | 0.0694–0.0905 | 0.42 | 2828 ± 35 | −16 | | |
| J16-Vgi-67–8 | <10 μm | None | AAR-32818.SI3.1 | 540 | 0–0.0176 | 0.35 | 1756 ± 35 | −20 | CI | 1777 ± 24 |
| Plaster | 11% | 9.5 ± 0.1 | AAR-32818.SI3.2 | 1260 | 0.0176–0.0353 | 0.35 | 1796 ± 34 | −18 | CI | (weighted average) |
| Stepwise injection | 185.2 mg | df=3 T=1.1(5% 7.8) | AAR-32818.SI3.3 | 2100 | 0.0353–0.0529 | 0.35 | 1964 ± 38 | −18 | | df=1 T=0.7(5% 3.8) |
| | | | AAR-32818.SI3.4 | 2850 | 0.0529–0.0695 | 0.33 | 2396 ± 34 | −19 | | |
| | | | AAR-32818.SI3.5 | 3780 | 0.0695–0.0891 | 0.38 | 2654 ± 32 | −13 | | |
| J16-Vgi-67–18 | <10 μm | Few | AAR-32819.SI1.1 | 240 | 0–0.0192 | 0.38 | 1491 ± 29 | −20 | | – |
| Plaster | 12% | 9.77 ± 0.02 | AAR-32819.SI1.1 | 720 | 0.0192–0.0392 | 0.40 | 1755 ± 32 | −11 | | – |
| Stepwise injection | 173.8 mg | df=3 T=15(5% 7.8) | AAR-32819.SI1.1 | 1560 | 0.0392–0.0667 | 0.55 | 2011 ± 29 | −15 | | |
| | | | AAR-32819.SI1.1 | 2040 | 0.0667–0.0922 | 0.51 | 2247 ± 32 | −13 | | |
| J16-Vgi-67–18 | <4 μm | None | AAR-32819.SI2.1 | 540 | 0–0.0157 | 0.32 | 1750 ± 33 | −15 | CIII + CIV | 1753 ± 24 |
| Plaster | 12% | 9.77 ± 0.02 | AAR-32819.SI2.2 | 1200 | 0.0157–0.0329 | 0.35 | 2003 ± 34 | −9 | (J16-Vgi-67–8, <10 μm) | (weighted average) |
| Stepwise injection | 166.4 mg | df=3 T=15(5% 7.8) | AAR-32819.SI2.3 | 1860 | 0.0329–0.0507 | 0.36 | 2097 ± 31 | −11 | | df=1 T=0.0(5% 3.8) |
| | | | AAR-32819.SI2.4 | 2580 | 0.0507–0.0689 | 0.37 | 2711 ± 34 | −10 | | |
| | | | AAR-32819.SI2.5 | 3420 | 0.0689–0.0904 | 0.43 | 2468 ± 35 | −10 | | |
| J16-Vi-26–24 | <4 μm | Few | AAR-32820.SI1.1 | 360 | 0–0.0199 | 0.40 | 2038 ± 32 | −17 | | – |
| Plaster | 11% | 9.80 ± 0.01 | AAR-32820.SI1.2 | 1050 | 0.0199–0.0370 | 0.35 | 2475 ± 34 | −11 | | – |
| Stepwise injection | 155.2 mg | df=3 T=14(5% 7.8) | AAR-32820.SI1.3 | 1890 | 0.0370–0.0533 | 0.33 | 2677 ± 35 | −13 | | |
| | | | AAR-32820.SI1.4 | 2640 | 0.0533–0.0723 | 0.39 | 2568 ± 33 | −14 | | |
| | | | AAR-32820.SI1.5 | 3510 | 0.0723–0.0922 | 0.40 | 2889 ± 33 | −13 | | |
| J16-Vi-26–24 | susp | Few | AAR-32820.SI2.1 | 420 | 0–0.0156 | 0.31 | 1839 ± 39 | −20 | | – |
| Plaster | 11% | 9.80 ± 0.01 | AAR-32820.SI2.2 | 1080 | 0.0156–0.0321 | 0.33 | 2193 ± 31 | −11 | | – |
| Stepwise injection | 174.4 mg | df=3 T=14(5% 7.8) | AAR-32820.SI2.3 | 1770 | 0.0321–0.0495 | 0.35 | 2745 ± 34 | −12 | | |
| | | | AAR-32820.SI2.4 | 2490 | 0.0495–0.0697 | 0.40 | 3398 ± 32 | −10 | | |
| J16-Vi-49–20 | susp | None | AAR-32821.SI1.1 | 330 | 0–0.0209 | 0.20 | 1167 ± 38 | −18 | CI | 1217 ± 46 |
| Plaster | 13% | 9.69 ± 0.02 | AAR-32821.SI1.2 | 810 | 0.0209–0.0420 | 0.20 | 1176 ± 40 | −12 | CI | (mean ± std) |
| Stepwise injection | 76.2 mg | df=3 T=3.7(5% 7.8) | AAR-32821.SI1.3 | 1650 | 0.0420–0.0612 | 0.18 | 1253 ± 38 | −11 | CI | df=3 T=5.5(5% 7.8) |
| | | | AAR-32821.SI1.4 | 2460 | 0.0612–0.0786 | 0.17 | 1271 ± 40 | −12 | CI | |
| Dalby001 | 46–75 μm** | N/A | AAR-17570.SD1.1 | N/A | 0–0.108 | N/A | 905 ± 25 | −18.11* | CIII + CIV | 915 ± 18 |
| Mortar | N/A | N/A | AAR-17570.SD1.2 | N/A | 0.108–0.305 | N/A | 1491 ± 28 | −9.23* | (Dalby009 (SD), 46–75 μm) | (weighted average) |
| Sequential dissolution | N/A | – | AAR-17570.SD1.3 | N/A | 0.305–0.522 | N/A | 2235 ± 25 | −8.00* | | df=1 T=0.4(5% 3.8) |
| Dalby001 | <10 μm | Medium | AAR-33415.SI1.1 | 360 | 0–0.00910 | 0.18 | 786 ± 40 | –22 | CI | 841 ± 39 |
| Mortar | 13% | 9.54 ± 0.02 | AAR-33415.SI1.2 | 960 | 0.00910–0.0209 | 0.24 | 872 ± 42 | −10 | CI | (mean ± std) |

(*continued on next page*)

**Table 1** (*continued*)

| Sample<br>Material<br>Preparation method | Grain fraction<br>Carbon yield (%)<br>Mass (mg) | CL orange-red grains<br>Alkalinity (pH)<br>$\chi^2$ test alkalinity | Laboratory no. | Reaction time (s) | Cumulative $CO_2$ fraction | Fraction mass (mgC) | $^{14}C$ age ($^{14}C$ years BP) | $\delta 13C_{AMS}$ (‰ VPDB) | Conclusiveness criteria | Conclusive age ($^{14}C$ years BP)<br>$\chi$2-test |
|---|---|---|---|---|---|---|---|---|---|---|
| Stepwise injection | 157.3 mg | df=3 T=2.5(5% 7.8) | AAR-33415.SI1.3 | 1590 | 0.0209–0.0357 | 0.30 | 865 ± 29 | −12 | CI | df=2 T=3.1(5% 6.0) |
| | | | AAR-33415.SI1.4 | 2160 | 0.0357–0.0538 | 0.36 | 952 ± 27 | −11 | | |
| Dalby009 | 46–75 μm** | N/A | AAR-17580.SD1.1 | N/A | 0–0.108 | N/A | 927 ± 27 | −17.31* | CI | 930 ± 18 |
| Mortar | N/A | N/A | AAR-17580.SD1.2 | N/A | 0.108–0.407 | N/A | 933 ± 25 | −11.16* | CI | (mean ± std) |
| Sequential dissolution | N/A | – | AAR-17580.SD1.3 | N/A | 0.407–0.537 | N/A | 1086 ± 25 | −10.03* | | df=1 T=0.0(5% 3.8) |
| Dalby009 | <10 μm | Medium | AAR-33416.SI1.1 | 360 | 0–0.0221 | 0.20 | 832 ± 37 | −16 | CI | 908 ± 45 |
| Mortar | 12% | 9.25 ± 0.09 | AAR-33416.SI1.2 | 930 | 0.0221–0.0440 | 0.20 | 941 ± 34 | −12 | CI | (mean ± std) |
| Stepwise injection | 163.6 mg | df=3 T=14(5% 7.8) | AAR-33416.SI1.3 | 1500 | 0.0440–0.0659 | 0.20 | 941 ± 40 | −13 | CI | df=3 T=5.9(5% 7.8) |
| | | (pH < references) | AAR-33416.SI1.4 | 2130 | 0.0659–0.0840 | 0.17 | 918 ± 43 | −13 | CI | |
| Fika057 | 46–75 μm** | Medium | AAR-10150.SD1.1 | N/A | 0–0.189 | N/A | 406 ± 35 | −10.5* | CI | 442 ± 31 |
| Mortar | 6.7% | N/A | AAR-10150.SD1.2 | N/A | 0.189–0.385 | N/A | 431 ± 30 | −10.4* | CI | (mean ± std) |
| Sequential dissolution | N/A | – | AAR-10150.SD1.3 | N/A | 0.385–0.579 | N/A | 485 ± 37 | −11.21* | CI | df=4 T=3.7(5% 9.5) |
| | | | AAR-10150.SD1.4 | N/A | 0.579–0.768 | N/A | 417 ± 35 | −11.68* | CI | |
| | | | AAR-10150.SD1.5 | N/A | 0.768–1 | N/A | 470 ± 34 | −11.23* | CI | |
| Fika057 | 46–75 μm** | Medium | AAR-33508.SI1.1 | 240 | 0–0.0205 | 0.33 | 438 ± 28 | −11 | CI | 446 ± 17 |
| Mortar | 6.7% | N/A | AAR-33508.SI1.2 | 720 | 0.0205–0.0457 | 0.40 | 458 ± 36 | −13 | CI | (weighted average) |
| Stepwise injection | 237.9 mg | – | AAR-33508.SI1.3 | 1170 | 0.0457–0.0661 | 0.32 | 448 ± 28 | −13 | CI | df=2 T=0.2(5% 6.0) |
| | | | AAR-33508.SI1.4 | 1680 | 0.0661–0.0855 | 0.31 | 543 ± 67 | −12 | | |
| Saka110 | <62 μm** | N/A | AAR-2998.SD1.1 | N/A | 0–0.44 | N/A | 620 ± 35 | −10.6* | | – |
| Mortar | N/A | N/A | AAR-2998.SD1.2 | N/A | 0.44–1 | N/A | 790 ± 40 | −9.5* | | – |
| Sequential dissolution | | – | | | | | | | | |
| Saka110 | 46–75 μm** | N/A | AAR-32213.SI1.1 | 900 | 0–0.0146 | 0.29 | 495 ± 36 | −17 | CI | 533 ± 35 |
| Mortar | 8.2% | N/A | AAR-32213.SI1.2 | 1830 | 0.0146–0.0302 | 0.31 | 524 ± 28 | −10 | CI | (mean ± std) |
| Stepwise injection | 244.3 mg | – | AAR-32213.SI1.3 | 2730 | 0.0302–0.0484 | 0.37 | 580 ± 27 | −13 | CI | df=2 T=4.1(5% 6.0) |
| | | | AAR-32213.SI1.4 | 3720 | 0.0484–0.0686 | 0.40 | 623 ± 26 | −12 | | |
| | | | AAR-32213.SI1.5 | 4710 | 0.0686–0.0878 | 0.39 | 661 ± 24 | −12 | | |
| TTK006 | 46–75 μm** | Medium | AAR-11094.SD1.1 | 17 | 0–0.0510 | N/A | 587 ± 35 | –22.4* | | – |
| Mortar | 10% | N/A | AAR-11094.SD1.2 | 80 | 0.0510–0.185 | N/A | 720 ± 35 | −8.9* | | – |
| Sequential dissolution | N/A | – | AAR-11094.SD1.3 | 240 | 0.185–0.446 | N/A | 1494 ± 35 | −10.8* | | |
| TTK006 | 21–45 μm** | N/A | AAR-29885.SI1.1 | 450 | 0–0.0143 | 0.38 | 743 ± 37 | −16 | CI | 722 ± 51 |
| Mortar | 10% | N/A | AAR-29885.SI1.2 | 1050 | 0.0143–0.0266 | 0.33 | 621 ± 37 | −14 | CI | (mean ± std) |
| Stepwise injection | 224 mg | – | AAR-29885.SI1.3 | 1700 | 0.0266–0.0396 | 0.35 | 764 ± 42 | −3 | CI | df=4 T=9.4(5% 9.5) |
| | | | AAR-29885.SI1.4 | 2310 | 0.0396–0.0536 | 0.37 | 743 ± 37 | −12 | CI | |
| | | | AAR-29885.SI1.5 | 2840 | 0.0536–0.0681 | 0.39 | 741 ± 33 | −15 | CI | |

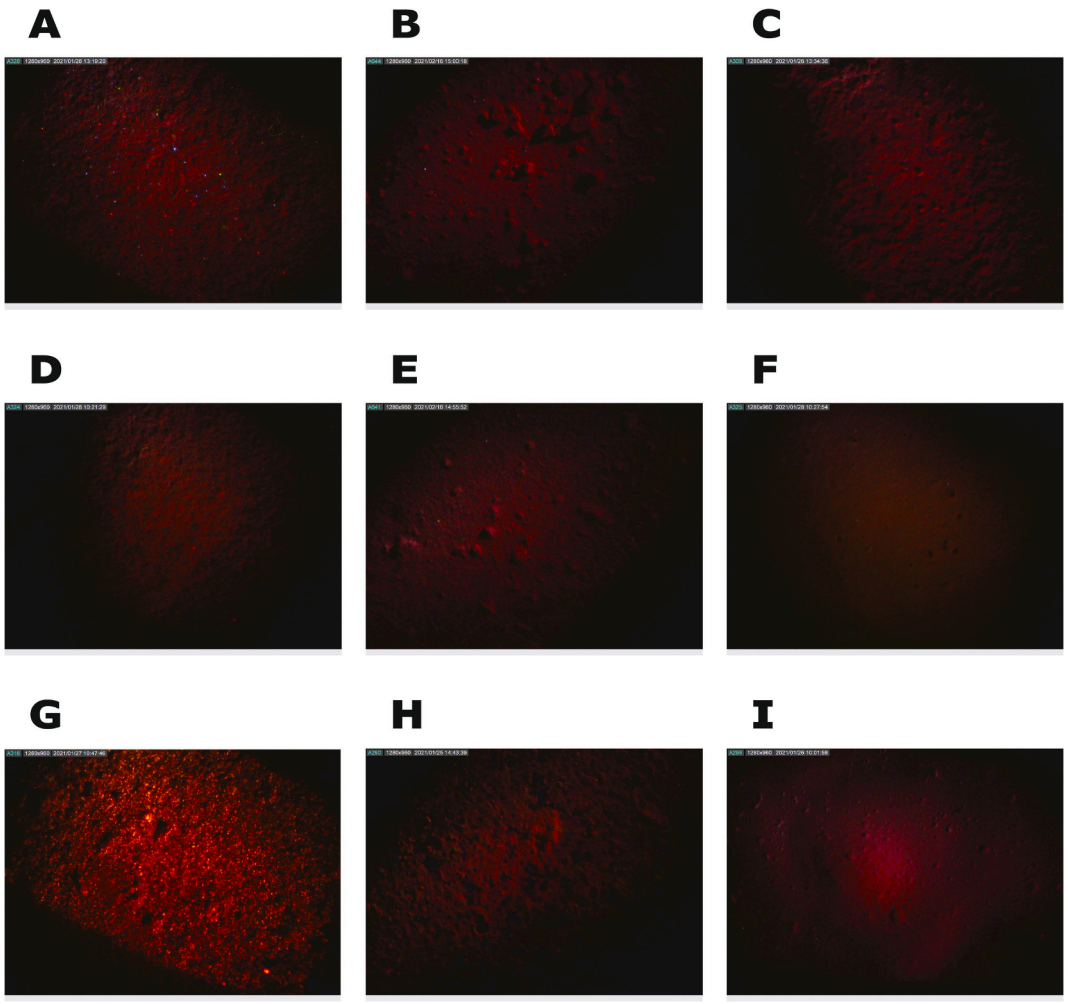


**Fig. 4.** CL microscopy where dark or dark-red is binder calcite, bright orange-red is limestone, blue is quartz, and green is feldspar. A-C J15-Pc-15-4 with grain fractions 38–63 μm, <38 μm and < 10 μm, respectively. D-F J16-Vgi-67-8 with grain fractions 38–63 μm, <38 μm and < 10 μm, respectively. G-H J15-Pc-28-2 with grain fractions 38–63 μm and < 4 μm, respectively. I J15-Pd-15-140 with < 4 μm grain fraction.

## 4. Discussion

### 4.1. Sample characterization

When cathodoluminescence identified orange-red grains, it was a valuable addition to understand radiocarbon profiles as a mixture of binder carbonate and more slowly dissolving geological carbonate. For the small grain fractions produced by sedimentation (<10 μm and < 4 μm) and cryo2sonic (susp) CL identified few or no orange-red grains. Surprisingly, there were a few examples where grain fractions with few or no orange-red grains in CL had radiocarbon profiles that were steeply older for later fractions, e.g. J15-Pd-15-140 and J16-Vi-26-24 in Fig. 6D, Fig. 6F and Table 1. It seemed that these powders could contain considerable geological carbonate while CL detected few orange-red grains, and this was reminiscent of Lichtenberger et al. (2015)'s non-luminescent limestone in Jerash mortar.

A pH-meter screened for alkalinity and its associated secondary carbonates. In Table 1, the samples J15-Pd-15-140, J16-Vgi-67-18 and J16-Vi-26-24 were alkaline, but it was uncertain to evaluate secondary carbonate's effect in the associated radiocarbon profiles because the effect of geological carbonate was also present, and the latter dominated and made later fractions increasingly older, see Fig. 6. As mentioned in the introduction, secondary carbonate dissolves the fastest so it mainly influences a profile's first fractions. As discussed below, the radiocarbon profile J15-Pa-16-100, <4 μm gave a conclusive age that was inaccurately too young. However, in Table 1 there is no indication that this sample was alkaline. There are ways for mortar and plaster to have secondary carbonates without alkalinity, though (Daugbjerg et al., 2021b).

### 4.2. Conclusiveness criteria

Sequential dissolution and stepwise injection produced results in the form of radiocarbon profiles; see Fig. 5, Fig. 6 and Table 1. Conclusiveness criteria then evaluated such profiles and ruled them either conclusive or inconclusive. Only conclusive radiocarbon profiles had derivation and presentation of sample age, see Table 1. This study's conclusiveness criteria are (Heinemeier et al., 2010; Ringbom et al., 2014; Lindroos et al., 2018):

CI: The $^{14}C$ ages of the first two, or more, $CO_2$ fractions from the same radiocarbon profile agree by a statistical test.

CII: The $^{14}C$ ages of the first fractions from three, or more, samples from the same building unit agree by a statistical test.

CIII: The $^{14}C$ ages of the first fractions from two samples from the same building unit agree by a statistical test. (Similar to CII but weaker)

CIV: The $^{14}C$ age of the first fraction from a sample agrees by a statistical test with another independent date (e.g. wood or charcoal) from the same building unit.

The used statistical test was a chi-square test for goodness of fit for the evaluated fractions' weighted average (Bennett and Franklin 1954;

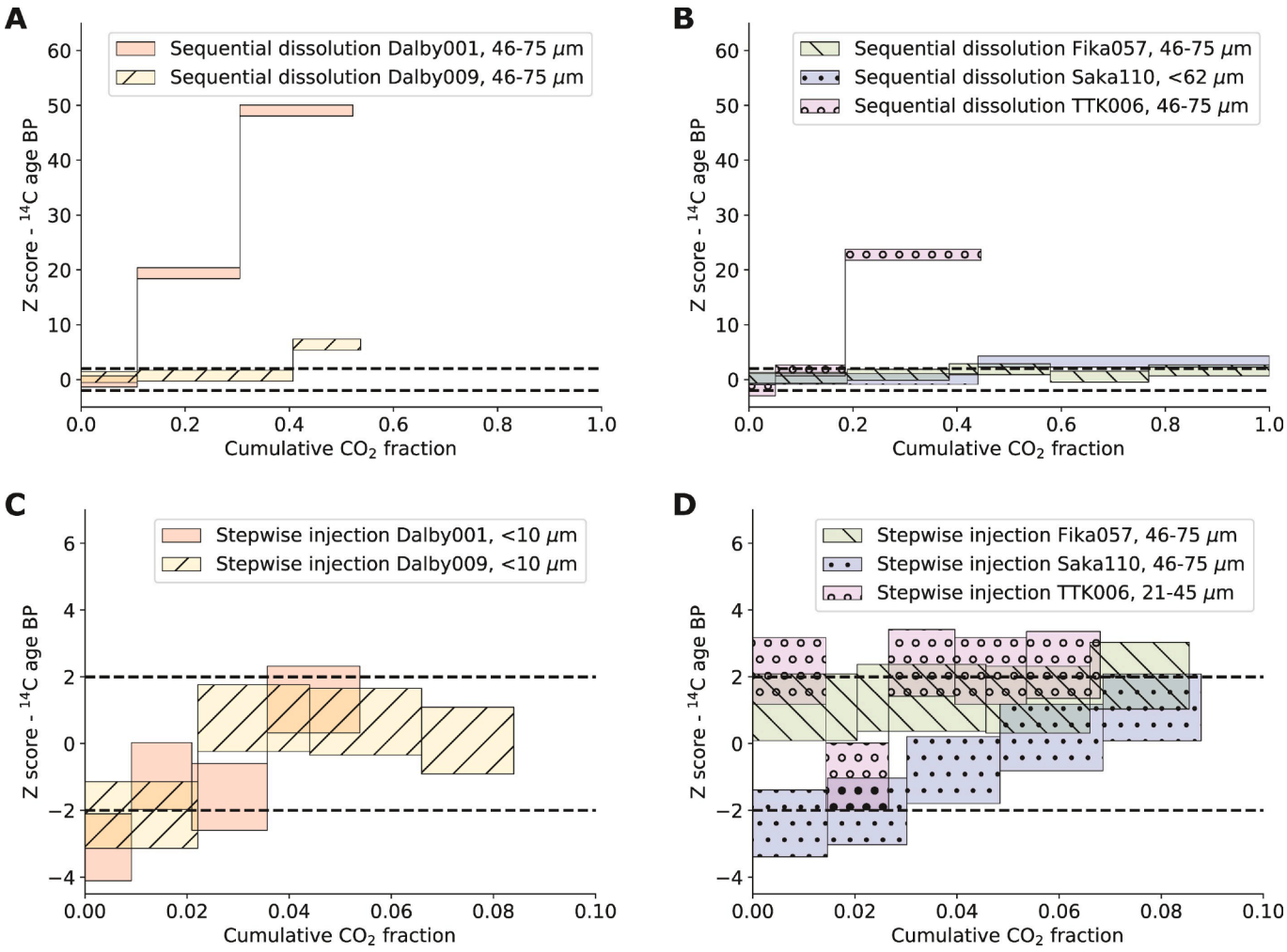


**Fig. 5.** Ordinates show Z scores for radiocarbon ages using the expected ages in Table 2. Abscissae show the cumulative fraction of $CO_2$ extracted from the sample, e.g. 0.02 means that the preparation has extracted 2% of the sample's carbon inventory as $CO_2$. For 'Stepwise injection Dalby001, <10 μm' Cumulative $CO_2$ fraction = 1 corresponded to 20 mgC. Sequential dissolution profiles for Dalby001 and Dalby009 were made by Lindroos et al. (2014) but unpublished. Sequential dissolution profiles for Fika057, Saka110 and TTK006 were quoted from Heinemeier et al. (2010) and Lindroos et al. (2011a). A Sequential dissolution for Dalby001 (46–75 μm) and Dalby009 (46–75 μm). B Sequential dissolution for Fika057 (46–75 μm), Saka110 (<62 μm) and TTK006 (46–75 μm). C Stepwise injection for Dalby001 (<10 μm) and Dalby009 (<10 μm). D Stepwise injection for Fika057 (46–75 μm), Saka110 (46–75 μm) and TTK006 (21–45 μm).

Press et al., 1992). For all fractions passing a criterion, there was calculated a weighted average with propagated uncertainty and a mean with standard deviation. If the propagated uncertainty was greater than the standard deviation, the conclusive age was the weighted average with propagated uncertainty. Else, the conclusive age was the mean with standard deviation. The fractions used in the conclusiveness criteria are in Table 1′s column 'Conclusiveness criteria', and the resulting conclusive mortar dates are in Table 1′s column 'Conclusive age'. Notice that the conclusiveness criteria can evaluate radiocarbon profiles for both known age samples and unknown age samples e.g. the Jerash samples.

The working assumption of the criteria is that in acid dissolution, secondary carbonates dissolve fastest, binder carbonate with a continuum from fast to slow dissolution rates and geological carbonate dissolve slowest (Lindroos et al., 2007; Heinemeier et al., 2010; Ringbom et al., 2014). With this assumption, an agreement among a number of first fractions indicates the absence of secondary- or geological-carbonate in these fractions. Conversely, distorted profiles without an agreement in first fractions indicate contamination with secondary- or geological-carbonate in these fractions. The discussion's subsection on mortar radiocarbon dates for known age samples, use the known age samples to evaluate the feasibility and accuracy of the conclusiveness criteria.

### 4.3. Mortar radiocarbon dates for known age samples

Comparing with sequential dissolution, the stepwise injection profiles in Fig. 5 extracted less of the total carbon inventory, and their fractions appeared to have more homogenous $^{14}C$ ages.

In Fig. 5, some first fractions of Dalby001 and Saka110 with stepwise injection were below the −2 Z score boundary. This indicated that stepwise injection, in some situations, picked up material younger than the hardening event, i.e. secondary carbonates had a significant effect on a very small portion of the carbon inventory. This could be a problem because profiles may pass conclusiveness criteria (see the discussion), while too young fractions influence the conclusive age's weighted average or mean. Considering this, we caution against using stepwise injection for unknown age mortar samples with secondary carbonates. It is possible that switching from diluted phosphoric acid to diluted hydrochloric acid will make stepwise injection less sensitive to secondary carbonates, as Hodgins et al. (2011) report this for pozzolana mortar.

In Fig. 5 and Table 1, the stepwise injection profiles for samples Dalby001, Dalby009, Fika057, Saka110 and TTK006 passed conclusiveness criterion CI (see the discussion), and Table 1 lists their conclusive ages. Table 2 compares conclusive ages and expected ages with a chi-square test for goodness of fit and Z-score, and Table 2 found

**Table 2**
Comparison of known age samples' conclusive age and expected age. Here all conclusive ages compared accurately. See the materials and methods section for the origin of the expected $^{14}$C ages.

| $^{14}$C Profile | Conclusiveness criterion and $\chi^2$ | Conclusive | Conclusive $^{14}$C age BP | Expected $^{14}$C age BP | $\chi^2$ of Conclusive $^{14}$C age BP and Expected $^{14}$C age BP | Z score of Conclusive $^{14}$C age BP and Expected $^{14}$C age BP | Accurate |
|---|---|---|---|---|---|---|---|
| Dalby001 (SD) | CIII, df=1 T=0.4(5% 3.8) | Yes | 915 ± 18 | 914 ± 10 | df=1 T=0.0(5% 3.8) | 0.1 | Yes |
| Dalby001 (SI) | CI, df=2 T=3.1(5% 6.0) | Yes | 841 ± 39 | 914 ± 10 | df=1 T=3.3(5% 3.8) | −1.8 | Yes |
| Dalby009 (SD) | CI, df=1 T=0.0(5% 3.8) | Yes | 930 ± 18 | 914 ± 10 | df=1 T=0.6(5% 3.8) | 0.8 | Yes |
| Dalby009 (SI) | CI, df=3 T=5.9(5% 7.8) | Yes | 908 ± 45 | 914 ± 10 | df=1 T=0.0(5% 3.8) | −0.1 | Yes |
| Fika057 (SD) | CI, df=4 T=3.7(5% 9.5) | Yes | 442 ± 31 | 391 ± 33 | df=1 T=1.3(5% 3.8) | 1.1 | Yes |
| Fika057 (SI) | CI, df=2 T=0.2(5% 6.0) | Yes | 446 ± 17 | 391 ± 33 | df=1 T=2.2(5% 3.8) | 1.5 | Yes |
| Saka110 (SD) | CI, df=1 T=10(5% 3.8) | No | – | 615 ± 35 | – | – | – |
| Saka110 (SI) | CI, df=2 T=4.1(5% 6.0) | Yes | 533 ± 35 | 615 ± 35 | df=1 T=2.7(5% 3.8) | −1.7 | Yes |
| TTK006 (SD) | CI, df=1 T=7.2(5% 3.8) | No | – | 659 ± 11 | – | – | – |
| TTK006 (SI) | CI, df=4 T=9.4(5% 9.5) | Yes | 722 ± 51 | 659 ± 11 | df=1 T=1.5(5% 3.8) | 1.2 | Yes |

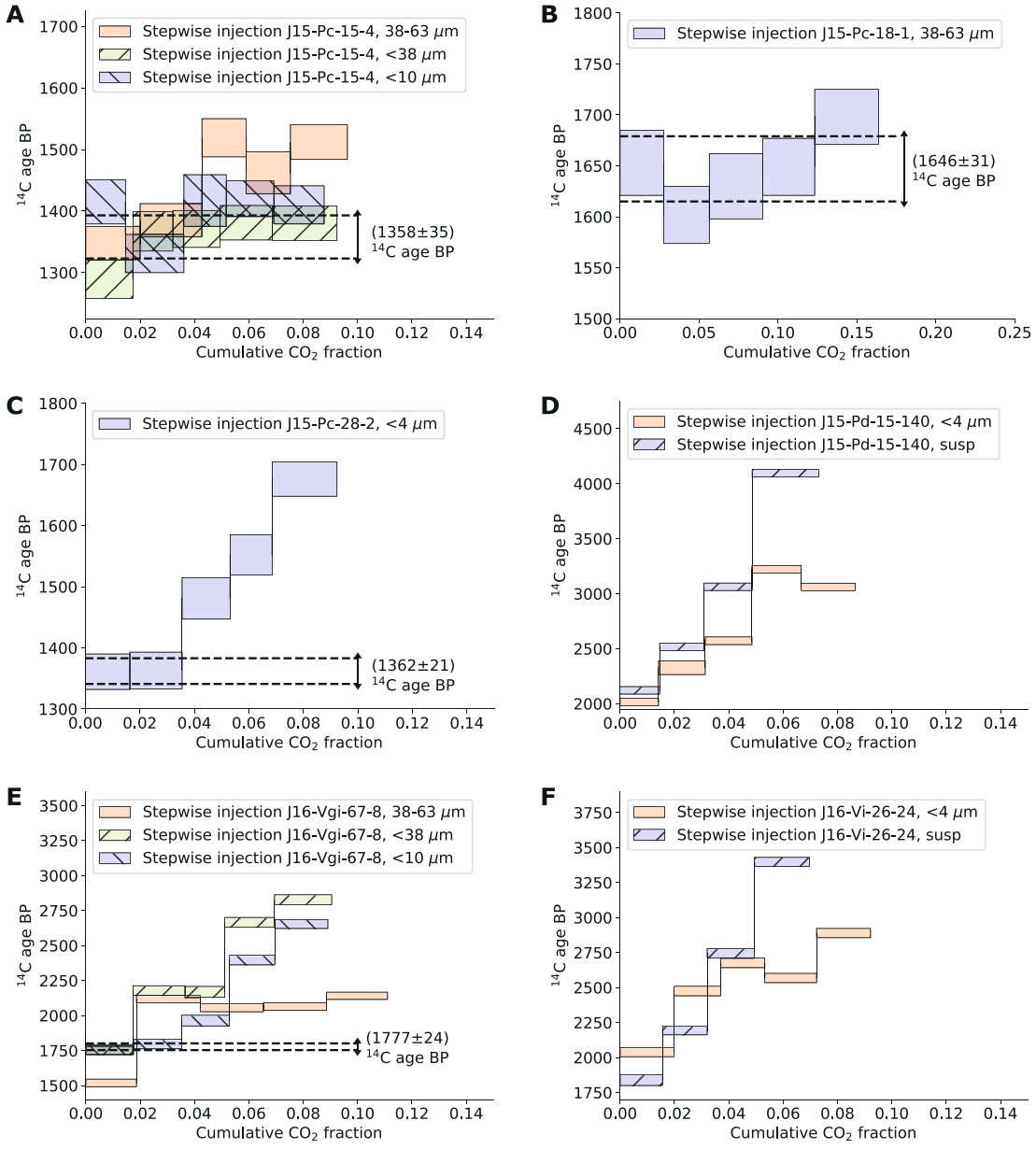


**Fig. 6.** Examples of radiocarbon profiles from the Umayyad house in trench P and V. Fractions' radiocarbon ages are shown as intervals with ± 1 standard deviation. A J15-Pc-15-4 with grain fractions 38–63 μm, <38 μm and < 10 μm. B J15-Pc-18-1 with grain fraction 38–63 μm. C J15-Pc-28-2 with grain fraction < 4 μm. D J15-Pd-15-140 with grain fractions < 4 μm and susp. E J16-Vgi-67-8 with grain fractions 38–63 μm, <38 μm and < 10 μm. F J16-Vi-26-24 with grain fractions < 4 μm and susp.

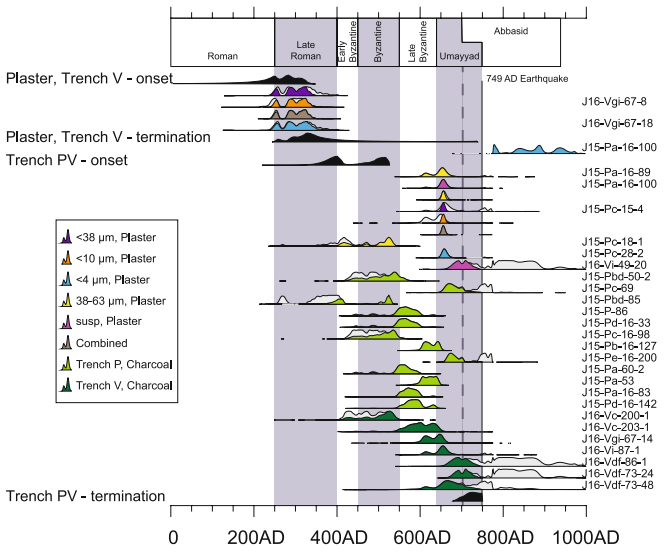


**Fig. 7.** Calibrated and modelled dates for the Umayyad house's radiocarbon dates. Conclusive plaster dates from Table 1. Charcoal dates from Philippsen and Olsen (2020).

accurate agreement. This supports the feasibility and soundness of using stepwise injection and the conclusiveness criteria as a methodology for radiocarbon dating lime mortar with geological carbonate. As such, the conclusiveness criteria are an empirical principle, supported by Table 2 and other studies (Heinemeier et al., 2010; Ringbom et al., 2014; Lindroos et al., 2018).

### 4.4. Plaster radiocarbon dates for the Umayyad house

Table 1 lists 8 inconclusive radiocarbon profiles, 9 CI dates, 1 CIII date and 2 CIII + CIV dates for the Umayyad house. To evaluate all conclusive mortar dates from trench P and V, two simple phase models were constructed. Model 1 consisted of the earliest ages from the plaster samples (J16-Vgi-67-8, J16-Vgi-67-18), and model 2 used the remaining plaster samples and charcoal samples from trench P and V (Fig. 7, Table 3) (Philippsen and Olsen, 2020). Plaster samples with $^{14}C$ ages from multiple methods were combined using the OxCal combine function.

The samples J15-Pc-18-1, J16-Vgi-67-8 and J16-Vgi-67-18 had age distributions covering Jerash's late Roman era (250–400 CE) and Byzantine era (400–640 CE) (See Thomsen (2019) for a Jerash chronology). It could be seen as surprising that plaster this old was found in relation to a house with all main phases attributed to Jerash's Umayyad era (Lichtenberger and Raja, 2017; Philippsen and Olsen, 2020). However, it is important to remember that the sampling picked loose plaster pieces, as explained in materials and methods. Earlier phases of building activity have been attested just south of the house dating to the Byzantine period. It is assumed that the street running in front of the house already existed in the 5th-6th centuries CE (Kalaitzoglou et al., forthcoming 1). In the Umayyad period, as well as in antiquity in general, older building materials from structures not in use anymore were often recycled as building materials and fill materials in new structures. Vitruvius, an ancient architect, presented a chapter on methods of building walls, which discussed broken material used as filling in walls:

*"But our workmen, in their hurry to finish, devote themselves only to the facings of the walls, setting them upright but filling the space between with a lot of broken stones and mortar thrown in anyhow."* (Vitruvius and Morgan 1914a).

In a chapter on floors, Vitruvius discussed broken and reused material for bedding of floors:

*"Then, upon this lay the bedding, composed of stones not smaller than can fill the hand. After the bedding is laid, mix the broken stone in the proportions, if it is new, of three parts to one of lime; if it is old material used again, five parts may answer to two in the mixture."* (Vitruvius and Morgan, 1914b).

There is plenty of evidence for reuse and recycling of materials in Jerash. In this study, Fig. 2F shows reuse of broken ceramics below plaster J15-Pd-15-140 in trench P. The plaster J15-Pc-18-1 sat on a ceramic water pipe, and this plaster date may suggest that the Umayyad house reused the water pipe. Other examples are a monumental block reused in a late antique oil press (Lichtenberger and Raja, 2015), a cistern reused for habitation (Lichtenberger et al., 2015), recycling of glass (Barfod, 2017; Barfod et al., 2018) and recycling of stones, mosaics and tesserae (Wootton, 2017).

The samples J15-Pa-16-89, J15-Pa-16-100 (susp), J15-Pc-15-4, J15-Pc-28-2 and J16-Vi-49-20 had calibrated date distributions overlapping with Jerash's Umayyad period (661–749 CE), with most of the probability at the beginning of the Umayyad period. The overall picture agreed with radiocarbon results of charcoal samples in trench P and V (Philippsen and Olsen, 2020) (see Fig. 7), and the discussion of archaeological evidence for the house's function and chronology (see the Introduction).

The sample J15-Pa-16-100 (<4 µm) had a calibrated date distribution after the 749 CE earthquake. As stated in the introduction, everything in the Umayyad house must date before the earthquake, and therefore the plaster date from J15-Pa-16-100, <4 µm, CI was inaccurate. Sample J15-Pa-16-100 was re-dated using the grain fraction, susp, and here it was accurately older than the earthquake (see Fig. 7 and Table 3). The pre-treatment of J15-Pa-16-100 (<4 µm) used a complete cross section of the stucco, ≈3.5 cm thick. Conversely, the pre-treatment for J15-Pa-16-100 (susp) chipped off the surface of the stucco, ≈1.0 cm thick. Considering the differences of thickness, the inaccuracy of J15-Pa-16-100 (<4 µm), CI may have been due to delayed hardening (Daugbjerg et al., 2021b).

### 4.5. Conclusiveness related to methodology

The appendix presents several tables. Table A1 compares the number of conclusive and inconclusive Jerash mortar and Jerash plaster dates in this study to the study by Lichtenberger et al. (2015). Of the two, this study had significantly more conclusive dates from Jerash, and a chi-square test of independence demonstrated this (Freedman et al., 2007; McHugh, 2013). Within the limits of Jerash lime plaster contaminated by geological carbonates, this data set can argue for using stepwise injection over sequential dissolution.

Table A2 presents conclusive and inconclusive plaster dates by the grain fractions produced by the pre-treatment methods. The chi-square test of independence passsed comparisons, and with this dataset, one cannot argue for a preferred grain fraction to optimize the number of conclusive dates.

Table A3 presents this study's conclusive and inconclusive plaster dates by different CL assessments. A chi-square test of independence found no significant differences between the CL assessments. However, it is interesting that for no orange-red grains in CL, 6 out of 7 radiocarbon profiles were conclusive. It is further interesting to consider using CL to screen against grain fractions with orange-red grains, though the insignificant test raised some questions over the effect hereof.

Table 1 shows 8 inconclusive radiocarbon profiles out of 20 for the Umayyad house. As such, Jerash mortar dating has room for further development, though stepwise injection was a significant improvement compared to sequential dissolution. The inconclusive radiocarbon profiles in Table 1 had late fractions that were hundreds of $^{14}C$ years to thousands of $^{14}C$ years older than expected for Jerash's Umayyad period, and most of the associated grain fractions had orange-red grains detected in CL (few or medium). With these considerations, geological carbonate is a likely explanation for these radiocarbon profiles being inconclusive. Stepwise injection performed better than sequential dissolution, but it was not immune to geological carbonate. It may be

**Table 3**
Calibrated and modelled dates for trench P and V radiocarbon dates. Charcoal dates from Philippsen and Olsen (2020).

| Lab ID | $^{14}$C Age ( $^{14}$C years BP) | Calibrated age 68.2% confidence interval(s) | Calibrated age 95.4% confidence interval(s) | Model agreement | Calibrated age (modelled) 68.2% confidence interval(s) | Calibrated age (modelled) 95.4% confidence interval(s) |
|---|---|---|---|---|---|---|
| MV_Early_Start | | | | | 207 CE – 327 CE [68.3%] | 184 BCE – 122 BCE [3.3%]<br>18 BC – 13 BC [0.2%]<br>11 BC – 339 CE [92.0%] |
| J16-Vgi-67–8, <38 μm, CIII, AAR-32818 | 1751 ± 23 | 250 CE – 262 CE [12.3%]<br>276 CE – 297 CE [20.1%]<br>309 CE – 346 CE [35.8%] | 242 CE – 366 CE [93.2%]<br>369 CE – 378 CE [2.3%] | 111.3% | 249 CE – 258 CE [13.0%]<br>282 CE – 298 CE [23.3%]<br>307 CE – 329 CE [32.0%]<br>251 CE – 257 CE [8.6%]<br>282 CE – 299 CE [24.9%]<br>307 CE – 329 CE [34.8%] | 242 CE – 262 CE [20.1%]<br>277 CE – 340 CE [75.3%]<br>244 CE – 261 CE [16.5%]<br>277 CE – 340 CE [78.9%] |
| J16-Vgi-67–8, <10 μm, CI, AAR-32818 | 1777 ± 24 | 243 CE – 256 CE [16.1%]<br>285 CE – 326 CE [52.2%] | 227 CE – 264 CE [27.1%]<br>275 CE – 348 CE [68.4%] | 104.0% | 249 CE – 258 CE [13.0%]<br>282 CE – 298 CE [23.3%]<br>307 CE – 329 CE [32.0%]<br>251 CE – 257 CE [8.6%]<br>282 CE – 299 CE [24.9%]<br>307 CE – 329 CE [34.8%] | 242 CE – 262 CE [20.1%]<br>277 CE – 340 CE [75.3%]<br>244 CE – 261 CE [16.5%]<br>277 CE – 340 CE [78.9%] |
| AAR-32818 | | 249 CE – 258 CE [13.0%]<br>282 CE – 298 CE [23.3%]<br>307 CE – 329 CE [32.0%] | 242 CE – 262 CE [20.1%]<br>277 CE – 340 CE [75.3%] | | 251 CE – 257 CE [8.6%]<br>282 CE – 299 CE [24.9%]<br>307 CE – 329 CE [34.8%] | 244 CE – 261 CE [16.5%]<br>277 CE – 340 CE [78.9%] |
| J16-Vgi-67–18, <4 μm, CIII, AAR-32819 | 1753 ± 24 | 249 CE – 262 CE [12.7%]<br>277 CE – 298 CE [20.6%]<br>307 CE – 345 CE [35.0%] | 241 CE – 366 CE [93.3%]<br>369 CE – 378 CE [2.1%] | 106.7% | 252 CE – 260 CE [8.8%]<br>278 CE – 299 CE [24.1%]<br>307 CE – 337 CE [35.3%] | 242 CE – 353 CE [94.7%]<br>357 CE – 361 CE [0.8%] |
| MV_Early_End | | | | | 255 CE – 264 CE [2.3%]<br>283 CE – 402 CE [65.9%] | 248 CE – 596 CE [92.3%]<br>601 CE – 603 CE [0.1%]<br>609 CE – 611 CE [0.1%]<br>687 CE – 690 CE [0.2%]<br>692 CE – 697 CE [0.2%]<br>698 CE – 738 CE [2.5%] |
| J15-Pa-16–100, <4 μm, CI, AAR-32814 | 1162 ± 23 | 776 CE – 787 CE [11.6%]<br>830 CE – 854 CE [17.1%]<br>874 CE – 895 CE [20.6%]<br>925 CE – 950 CE [19.0%] | 775 CE – 790 CE [13.0%]<br>807 CE – 810 CE [0.4%]<br>821 CE – 902 CE [52.1%]<br>915 CE – 976 CE [29.9%] | 99.8% | 776 CE – 787 CE [11.4%]<br>830 CE – 854 CE [17.1%]<br>874 CE – 895 CE [20.5%]<br>925 CE – 950 CE [19.2%] | 775 CE – 790 CE [12.9%]<br>806 CE – 809 CE [0.5%]<br>821 CE – 903 CE [52.0%]<br>915 CE – 976 CE [30.1%] |
| PV_start | | | | | 372 CE – 411 CE [37.4%]<br>490 CE – 524 CE [30.8%] | 342 CE – 420 CE [49.3%] |
| J15-Pa-16–89, 38–63 μm, CIII, AAR-32813 | 1382 ± 35 | 609 CE – 621 CE [12.2%]<br>640 CE – 668 CE [56.0%] | 600 CE – 683 CE [90.6%]<br>745 CE – 760 CE [3.8%]<br>767 CE – 772 CE [1.0%] | 105.6% | 610 CE – 618 CE [9.6%]<br>640 CE – 668 CE [58.7%] | 602 CE – 679 CE [95.4%] |
| J15-Pa-16–100, susp, CI, AAR-32814 | 1373 ± 26 | 646 CE – 666 CE [68.3%] | 606 CE – 627 CE [8.3%]<br>636 CE – 679 CE [84.8%]<br>750 CE – 758 CE [2.1%]<br>769 CE – 771 CE [0.3%] | 104.1% | 647 CE – 665 CE [68.3%] | 607 CE – 625 CE [7.8%]<br>638 CE – 678 CE [87.6%] |
| J15-Pc-15–4, 38–63 μm, CI, AAR-32815 | 1367 ± 19 | 651 CE – 664 CE [68.3%] | 643 CE – 675 CE [95.4%] | 117.4% | 652 CE – 660 CE [68.3%]<br>651 CE – 660 CE [68.3%] | 648 CE – 665 CE [95.4%]<br>647 CE – 665 CE [95.4%] |
| J15-Pc-15–4, <38 μm, CI, AAR-32815 | 1358 ± 35 | 645 CE – 679 CE [57.7%]<br>750 CE – 759 CE [8.3%]<br>769 CE – 772 CE [2.3%] | 606 CE – 627 CE [5.4%]<br>637 CE – 705 CE [69.7%]<br>740 CE – 773 CE [20.4%] | 165.7% | 652 CE – 660 CE [68.3%]<br>651 CE – 660 CE [68.3%] | 648 CE – 665 CE [95.4%]<br>647 CE – 665 CE [95.4%] |
| J15-Pc-15–4, <10 μm, CI, AAR-32815 | 1399 ± 34 | 607 CE – 624 CE [24.1%]<br>638 CE – 660 CE [44.1%] | 594 CE – 673 CE [95.4%] | 119.9% | 652 CE – 660 CE [68.3%]<br>651 CE – 660 CE [68.3%] | 648 CE – 665 CE [95.4%]<br>647 CE – 665 CE [95.4%] |
| AAR-32815 | | 652 CE – 660 CE [68.3%] | 648 CE – 665 CE [95.4%] | | 651 CE – 660 CE [68.3%] | 647 CE – 665 CE [95.4%] |
| J15-Pc-18–1, 38–63 μm, CI, AAR-32812 | 1646 ± 31 | 381 CE – 436 CE [47.5%]<br>465 CE – 476 CE [6.6%]<br>500 CE – 510 CE [5.1%]<br>516 CE – 531 CE [9.1%] | 264 CE – 274 CE [2.5%]<br>350 CE – 482 CE [72.1%]<br>492 CE – 538 CE [20.9%] | 91.2% | 408 CE – 428 CE [15.7%]<br>499 CE – 537 CE [52.6%] | 389 CE – 442 CE [26.4%]<br>450 CE – 482 CE [10.7%]<br>487 CE – 543 CE [58.3%] |
| J15-Pc-28–2, <4 μm, CI, AAR-32816 | 1362 ± 21 | 651 CE – 666 CE [68.3%] | | 104.5% | 652 CE – 666 CE [68.3%] | 645 CE – 677 CE [95.4%] |

(*continued on next page*)

**Table 3** (*continued*)

| Lab ID | $^{14}$C Age ($^{14}$C years BP) | Calibrated age 68.2% confidence interval(s) | Calibrated age 95.4% confidence interval(s) | Model agreement | Calibrated age (modelled) 68.2% confidence interval(s) | Calibrated age (modelled) 95.4% confidence interval(s) |
|---|---|---|---|---|---|---|
| | | | 643 CE – 680 CE [92.2%]<br>750 CE – 759 CE [2.8%]<br>769 CE – 771 CE [0.4%] | | | |
| J16-Vi-49–20, susp, CI, AAR-32821 | 1217 ± 46 | 707 CE – 725 CE [7.9%]<br>774 CE – 777 CE [1.6%]<br>781 CE – 883 CE [58.8%] | 674 CE – 754 CE [24.0%]<br>757 CE – 896 CE [67.9%]<br>925 CE – 950 CE [3.6%] | 67.1% | 680 CE – 700 CE [36.4%]<br>702 CE – 720 CE [31.8%] | 668 CE – 736 CE [95.4%] |
| J15-Pbd-50–2 SPL101 AAR-24336 | 1572 ± 27 | 435 CE – 466 CE [25.7%]<br>475 CE – 501 CE [22.6%]<br>508 CE – 517 CE [6.8%]<br>530 CE – 546 CE [13.2%] | 426 CE – 561 CE [95.4%] | 95.6% | 480 CE – 555 CE [68.3%] | 433 CE – 568 CE [95.4%] |
| J15-Pc-69 SPL248 AAR-23931 | 1319 ± 36 | 660 CE – 688 CE [31.4%]<br>698 CE – 702 CE [3.9%]<br>742 CE – 773 CE [33.0%] | 653 CE – 709 CE [49.4%]<br>712 CE – 774 CE [46.0%] | 99.3% | 658 CE – 690 CE [63.1%]<br>698 CE – 702 CE [5.2%] | 650 CE – 730 CE [95.4%] |
| J15-Pbd-85 AAR-23933 | 1697 ± 26 | 265 CE – 273 CE [8.1%]<br>350 CE – 406 CE [60.2%] | 258 CE – 282 CE [17.3%]<br>329 CE – 417 CE [78.2%] | 49.9% | 392 CE – 417 CE [35.4%]<br>516 CE – 532 CE [32.8%] | 366 CE – 425 CE [48.7%]<br>468 CE – 475 CE [1.6%]<br>498 CE – 536 CE [45.2%] |
| J15-P-86 SPL171 AAR-24341 | 1520 ± 28 | 545 CE – 593 CE [68.3%] | 437 CE – 463 CE [5.4%]<br>476 CE – 500 CE [6.5%]<br>510 CE – 516 CE [0.6%]<br>532 CE – 606 CE [81.4%]<br>625 CE – 637 CE [1.6%] | 104.7% | 546 CE – 591 CE [68.3%] | 440 CE – 451 CE [1.6%]<br>454 CE – 461 CE [0.7%]<br>478 CE – 499 CE [4.2%]<br>510 CE – 516 CE [0.6%]<br>531 CE – 607 CE [86.6%]<br>625 CE – 637 CE [1.8%] |
| J15-Pd-16–33 SPL79 AAR-29112 | 1523 ± 26 | 544 CE – 590 CE [68.3%] | 437 CE – 463 CE [5.5%]<br>476 CE – 500 CE [6.7%]<br>510 CE – 516 CE [0.6%]<br>531 CE – 605 CE [82.6%] | 105.0% | 545 CE – 587 CE [68.3%] | 440 CE – 452 CE [1.7%]<br>455 CE – 461 CE [0.7%]<br>478 CE – 499 CE [4.4%]<br>510 CE – 516 CE [0.6%]<br>531 CE – 606 CE [87.6%]<br>630 CE – 634 CE [0.5%] |
| J15-Pc-16–98 SPL152 AAR-29114 | 1582 ± 21 | 435 CE – 466 CE [28.1%]<br>475 CE – 501 CE [23.2%]<br>507 CE – 517 CE [8.4%]<br>530 CE – 540 CE [8.6%] | 427 CE – 546 CE [95.4%] | 96.0% | 479 CE – 482 CE [2.0%]<br>483 CE – 547 CE [66.2%] | 431 CE – 552 CE [95.4%] |
| J15-Pb-16–127 SPL165 AAR-29115 | 1428 ± 19 | 606 CE – 626 CE [43.5%]<br>637 CE – 648 CE [24.8%] | 601 CE – 652 CE [95.4%] | 99.9% | 606 CE – 626 CE [43.5%]<br>637 CE – 648 CE [24.7%] | 601 CE – 652 CE [95.4%] |
| J15-Pe-16–200 SPL214 AAR-29121 | 1310 ± 21 | 666 CE – 686 CE [28.8%]<br>743 CE – 762 CE [28.5%]<br>765 CE – 773 CE [10.9%] | 659 CE – 707 CE [47.9%]<br>727 CE – 732 CE [1.2%]<br>737 CE – 774 CE [46.4%] | 91.3% | 664 CE – 689 CE [65.5%]<br>699 CE – 701 CE [2.8%] | 656 CE – 709 CE [93.9%]<br>726 CE – 730 CE [0.8%]<br>741 CE – 745 CE [0.8%] |
| J15-Pa-60–2 SPL256 AAR-29123 | 1529 ± 22 | 542 CE – 582 CE [68.3%] | 439 CE – 462 CE [5.3%]<br>478 CE – 498 CE [7.0%]<br>533 CE – 601 CE [83.1%] | 105.1% | 542 CE – 579 CE [68.3%] | 441 CE – 451 CE [1.5%]<br>456 CE – 460 CE [0.4%]<br>478 CE – 498 CE [4.7%]<br>532 CE – 602 CE [88.8%] |
| J15-Pa-53 SPL102 AAR-29126 | 1445 ± 19 | 604 CE – 612 CE [15.5%]<br>615 CE – 641 CE [52.8%] | 590 CE – 650 CE [95.4%] | 100.0% | 604 CE – 612 CE [15.3%]<br>613 CE – 614 CE [1.5%]<br>615 CE – 616 CE [1.0%]<br>617 CE – 641 CE [50.4%] | 590 CE – 650 CE [95.4%] |
| J15-Pa-16–83 SPL156 AAR-29145 | 1507 ± 21 | 560 CE – 595 CE [68.3%] | 542 CE – 605 CE [94.5%]<br>629 CE – 634 CE [1.0%] | 100.5% | 559 CE – 595 CE [68.3%] | 542 CE – 605 CE [95.0%]<br>630 CE – 634 CE [0.5%] |
| J15-Pd-16–142 SPL199 AAR-29146 | 1492 ± 25 | 563 CE – 604 CE [68.3%] | 546 CE – 610 CE [83.6%]<br>618 CE – 640 CE [11.9%] | 100.3% | 563 CE – 603 CE [68.3%] | 547 CE – 610 CE [83.8%]<br>619 CE – 640 CE [11.7%] |
| J16-Vc-200–1 SPL225 AAR-25882 | 1612 ± 31 | 418 CE – 440 CE [19.1%]<br>452 CE – 455 CE [2.2%]<br>461 CE – 478 CE [15.1%]<br>497 CE – 535 CE [31.9%] | 411 CE – 544 CE [95.4%] | 100.7% | 427 CE – 428 CE [0.3%]<br>432 CE – 433 CE [0.5%]<br>465 CE – 478 CE [7.3%]<br>494 CE – 543 CE [60.2%] | 417 CE – 547 CE [95.4%] |
| J16-Vc-203–1 SPL220 AAR-25879 | 1470 ± 40 | | 544 CE – 652 CE [95.4%] | 100.9% | | 547 CE – 651 CE [95.4%] |

(*continued on next page*)

**Table 3** (*continued*)

| Lab ID | $^{14}$C Age ($^{14}$C years BP) | Calibrated age 68.2% confidence interval(s) | Calibrated age 95.4% confidence interval(s) | Model agreement | Calibrated age (modelled) 68.2% confidence interval(s) | Calibrated age (modelled) 95.4% confidence interval(s) |
|---|---|---|---|---|---|---|
| | | 573 CE – 611 CE [42.9%] | | | 573 CE – 610 CE [42.7%] | |
| | | 618 CE – 641 CE [25.3%] | | | 617 CE – 641 CE [25.6%] | |
| J16-Vgi-67–14 SPL179 AAR-25877 | 1409 ± 35 | 606 CE – 627 CE [32.1%] | 588 CE – 668 CE [95.4%] | 100.6% | 606 CE – 627 CE [32.1%] | 590 CE – 667 CE [95.4%] |
| | | 637 CE – 656 CE [36.1%] | | | 637 CE – 656 CE [36.2%] | |
| J16-Vi-87–1 SPL211 AAR-25878 | 1377 ± 35 | 610 CE – 620 CE [8.8%] | 601 CE – 686 CE [88.1%] | 107.4% | 612 CE – 617 CE [5.5%] | 603 CE – 682 CE [95.4%] |
| | | 640 CE – 671 CE [59.4%] | 744 CE – 761 CE [5.6%] | | 641 CE – 670 CE [62.7%] | |
| | | | 766 CE – 773 CE [1.8%] | | | |
| J16-Vdf-86–1 SPL230 AAR-25883 | 1218 ± 62 | 691 CE – 696 CE [1.4%] | 668 CE – 900 CE [86.1%] | 82.1% | 675 CE – 717 CE [68.3%] | 661 CE – 737 CE [95.4%] |
| | | 704 CE – 741 CE [14.6%] | 918 CE – 963 CE [8.1%] | | | |
| | | 773 CE – 887 CE [52.3%] | 965 CE – 975 CE [1.3%] | | | |
| J16-Vdf-73–24 SPL231 AAR-25884 | 1215 ± 39 | 710 CE – 712 CE [1.0%] | 679 CE – 747 CE [19.7%] | 54.4% | 683 CE – 699 CE [31.1%] | 672 CE – 736 CE [95.4%] |
| | | 774 CE – 777 CE [1.5%] | 759 CE – 768 CE [1.2%] | | 703 CE – 722 CE [37.2%] | |
| | | 781 CE – 882 CE [65.8%] | 772 CE – 894 CE [72.5%] | | | |
| | | | 928 CE – 946 CE [2.0%] | | | |
| J16-Vdf-73–48 SPL264 AAR-25902 | 1334 ± 62 | 648 CE – 707 CE [39.1%] | 600 CE – 776 CE [87.2%] | 105.7% | 647 CE – 706 CE [68.3%] | 602 CE – 735 CE [95.4%] |
| | | 727 CE – 774 CE [29.2%] | 787 CE – 830 CE [6.5%] | | | |
| | | | 855 CE – 874 CE [1.7%] | | | |
| PV_End | | | | | 714 CE – 749 CE [68.3%] | 693 CE – 750 CE [95.4%] |

possible to obtain some further increase of the number of conclusive radiocarbon profiles by screening against grain fractions with orange-red grains in CL.

## 5. Conclusion

This study attempted to advance methodologies for Jerash mortar dating, whose main challenge is contamination from geological carbonate. With Jerash plaster samples, stepwise injection produced 12 conclusive profiles and 8 inconclusive profiles out of 20 complete profiles. Of the 12 conclusive profiles, 11 were accurately younger than the 749 CE earthquake. The 8 inconclusive profiles showed signs of persisting contamination from geological carbonate, and there remains room for further methodological development. For known age samples from Finland and Sweden, 5 out of 5 radiocarbon profiles passed conclusiveness criteria and accurately matched the expected ages.

The discussion evaluated supposed connections between conclusiveness and mortar dating methodology with chi-square tests of independence. Stepwise injection and Jerash samples (this study) had significantly more conclusive radiocarbon profiles, than sequential dissolution and Jerash samples (Lichtenberger et al., 2015). In addition, grain fractions with no orange-red grains in CL had 6 out of 7 conclusive radiocarbon profiles. With this interesting result, one could imagine a stricter CL screening before mortar radiocarbon dating. However, this result tested statistically insignificant, so within this dataset there was some doubt about the effect of CL screening.

Overall, this study was a significant improvement for Jerash mortar dating compared to the previous study by Lichtenberger et al. (2015). An important reason for this improvement was that stepwise injection focused on the crucial first 10% of dissolved carbonate. Seven plaster dates supported the construction of the Umayyad house in the Umayyad era. Four plaster dates suggested the reuse of pre-Umayyad material in the Umayyad house. One plaster date inaccurately suggested a radiocarbon date after the 749 CE earthquake.

### *CRediT authorship contribution statement*

**Thomas Schrøder Daugbjerg:** Conceptualization, Methodology, Investigation, Formal analysis, Writing – original draft, Writing – review & editing, Visualization. **Achim Lichtenberger:** Conceptualization, Resources, Project administration, Funding acquisition, Writing – review & editing. **Alf Lindroos:** Conceptualization, Resources, Investigation, Writing – review & editing. **Rubina Raja:** Conceptualization, Resources, Writing – review & editing, Project administration, Funding acquisition. **Jesper Olsen:** Conceptualization, Supervision, Writing – review & editing, Project administration.


## Acknowledgements

The work of the Danish-German Jerash Northwest Quarter Project was supported by the Carlsberg Foundation, the Danish National Research Foundation under the grant DNRF119 – Centre of Excellence for Urban Network Evolutions (UrbNet), Deutsche Forschungsgemeinschaft, Deutscher Palästina-Verein, the EliteForsk initiative of the Danish Ministry of Higher Education and Science and H. P. Hjerl Hansens Mindefondet for Dansk Palæstinaforskning. Thanks to Heikki Ranta for providing us the two samples from Dalby church.


## Appendix

Table A1, Table A2 and Table A3 organize this study's numbers of conclusive and inconclusive radiocarbon profiles for comparison with Lichtenberger et al. (2015)'s results, grain fractions and cathodoluminescence results. Information from this study derived from Table 1. This appendix re-evaluated Lichtenberger et al. (2015)'s radiocarbon profiles as conclusive or inconclusive considering their

discussion and uniformity with this study's conclusiveness criteria. This found 7 conclusive and 20 inconclusive radiocarbon profiles in Lichtenberger et al. (2015). For each table, a chi-square test of independence (Freedman et al., 2007; McHugh, 2013) assumed the null hypothesis that the rows had similar observed numbers of conclusive and inconclusive results. Accordingly, expected numbers were calculated by multiplying a study's number of radiocarbon profiles (observed row sum) with the ratio of all conclusive, or inconclusive, profiles (observed column sum) to all profiles (sum of the entire observed table). E.g. Lichtenberger et al. (2015)'s expected number of conclusive radiocarbon profiles was 27·19/47 = 10.9. A $\chi^2_{Test}$ value was calculated from the observed and expected numbers, and comparison with a $\chi^2_{Critical}$ value rejected ($\chi^2_{Test} > \chi^2_{Critical}$), or failed to reject ($\chi^2_{Test} \leq \chi^2_{Critical}$), the null hypothesis. Here $\chi^2_{Critical}$ was calculated using significance level, α = 0.05, and degrees of freedom, df = (m-1)·(n-1), where m was the number of observed rows and n was the number of observed columns.

**Table A1**
This table compares Lichtenberger et al. (2015)'s and this study's numbers of conclusive and inconclusive radiocarbon profiles from Jerash mortar and plaster. See the appendix for an explanation of the expected numbers. Null hypothesis: the two studies had similar observed numbers of conclusive and inconclusive radiocarbon profiles. Chi-square test of independence: rejected the null hypothesis ($\chi^2_{Test} > \chi^2_{Critical}$). Conclusion: this study had significantly more conclusive Jerash radiocarbon profiles than Lichtenberger et al. (2015).

| | Observed (O) | | Expected (E) | |
|---|---|---|---|---|
| | Conclusive | Inconclusive | Conclusive | Inconclusive |
| Lichtenberger et al. (2015) | 7 | 20 | 10.9 | 16.1 |
| This study (Jerash) | 12 | 8 | 8.1 | 11.9 |
| $\chi^2_{Test} = \Sigma(O\text{-}E)^2/E$ | | | | 5.5 |
| $\chi^2_{Critical}$ | | | | $\chi^2(df = 1, \alpha = 5\%) = 3.8$ |

**Table A2**
Comparison of this study's conclusive and inconclusive radiocarbon profiles by various grain fractions. See the appendix for an explanation of the expected numbers. Null hypothesis: the grain fractions had similar observed numbers of conclusive and inconclusive radiocarbon profiles. Chi-square test of independence: failed to reject the null hypothesis ($\chi^2_{Test} \leq \chi^2_{Critical}$). Conclusion: the dataset had insignificant differences regarding conclusive and inconclusive results between the grain fractions.

| | Observed (O) | | Expected (E) | |
|---|---|---|---|---|
| Grain fraction | Conclusive | Inconclusive | Conclusive | Inconclusive |
| 38–63 μm | 3 | 1 | 2.4 | 1.6 |
| <38 μm | 2 | 1 | 1.8 | 1.2 |
| <10 μm | 2 | 1 | 1.8 | 1.2 |
| <4 μm | 3 | 3 | 3.6 | 2.4 |
| susp | 2 | 2 | 2.4 | 1.6 |
| $\chi^2_{Test} = \Sigma(O\text{-}E)^2/E$ | | | | 0.9 |
| $\chi^2_{Critical}$ | | | | $\chi^2(df = 4, \alpha = 5\%) = 9.5$ |

**Table A3**
Conclusive and inconclusive radiocarbon profiles by cathodoluminescence results. 'Few' and 'Medium' from Table 1 were grouped to one row 'Detected'. See the appendix for an explanation of the expected numbers. Null hypothesis: the cathodoluminescence results had similar observed numbers of conclusive and inconclusive radiocarbon profiles. Chi-square test of independence: failed to reject the null hypothesis ($\chi^2_{Test} \leq \chi^2_{Critical}$). Conclusion: the dataset had insignificant differences regarding conclusive and inconclusive results between the cathodoluminescence results.

| | Observed (O) | | Expected (E) | |
|---|---|---|---|---|
| Orange-red grains in cathodoluminescence | Conclusive | Inconclusive | Conclusive | Inconclusive |
| None | 6 | 1 | 4.2 | 2.8 |
| Detected | 6 | 7 | 7.8 | 5.2 |
| $\chi^2_{Test} = \Sigma(O\text{-}E)^2/E$ | | | | 3.0 |
| $\chi^2_{Critical}$ | | | | $\chi^2(df = 1, \alpha = 5\%) = 3.8$ |

## References


Al-Bashaireh, K., Hodgins, G.W., 2012. Lime mortar and plaster: a radiocarbon dating tool for dating nabatean structures in Petra, Jordan. Radiocarbon 54 (3-4), 905–914.

Al-Bashaireh, K., 2013. Plaster and mortar radiocarbon dating of nabatean and islamic structures, South Jordan. Archaeometry 55 (2), 329–354.

Al-Bashaireh, K., 2015. Radiocarbon age determinations of mosaic mortar layers of churches from north Jordan. Radiocarbon 57 (5), 851–863.

Barfod, G., Freestone, I., Lichtenberger, A., Raja, R., Schwarzer, H., 2018. Geochemistry of Byzantine and Early Islamic glass from Jerash, Jordan: Typology, recycling, and provenance. Geoarchaeology.

Barfod, G.H., Larsen, J.M., Lichtenberger, A., Raja, R., 2015. Revealing text in a complexly rolled silver scroll from Jerash with computed tomography and advanced imaging software. Sci. Rep. 5 (1), 17765.

Barfod, G.H., 2017. "Recycling, reuse and reduce": glass in ancient Gerasa. In: Lichtenberger A, Raja R, editors. Gerasa/Jerash: from the Urban Periphery. Aarhus. p 115-8.

Barrett, G.T., Donnelly, C., Reimer, P.J., 2020. Radiocarbon dating mortar: the identification of a medieval Irish round tower using a multi-method inter-comparative approach. J. Archaeolog. Sci.: Rep. 33, 102538. https://doi.org/10.1016/j.jasrep.2020.102538.

Bennett, C.A., Franklin, N.L., 1954. Statistical analysis in chemistry and the chemical industry. New York: Wiley.

Bronk Ramsey, C., 2009. Bayesian analysis of radiocarbon dates. Radiocarbon 51(1):337-60.

Brown, T.A., Southon, J.R., 1997. Corrections for contamination background in AMS 14C measurements. Nuclear Instruments and Methods in Physics Research Section B: Beam Interactions with Materials and Atoms 123(1):208 - 13.

Daugbjerg, T.S., Lindroos, A., Hajdas, I., Ringbom, Å., Olsen, J., 2021a. Comparison of thermal decomposition and sequential dissolution—two sample preparation methods for radiocarbon dating of lime mortars. Radiocarbon 63(2):405-27.

Daugbjerg, T.S., Lindroos, A., Heinemeier, J., Ringbom, Å., Barrett, G., Michalska, D., Hajdas, I., Raja, R., Olsen, J., 2021b. A field guide to mortar sampling for radiocarbon dating*. Archaeometry.

Donahue, D.J., Linick, T.W., Jull, A.J.T., 1990. Isotope-ratio and background corrections for accelerator mass spectrometry radiocarbon measuments. Radiocarbon 32:135-42.

EMD Millipore, 2013. Milli-Q® Integral Water Purification Systems. Darmstadt, Germany: Merck KGaA.

Folk, R.L., Valastro, S., 1976. Successful technique for dating of lime mortar by carbon-14. J. Field Archaeol. 3 (2), 195–201.

Freedman, D., Pisana, R., Purves, R., 2007. Statistics. New York: W. W. Norton & Company, Inc.

Gardberg, C.J., Heininen, S., Welin, P.O., 2000. Nationalhelgedomen. Åbo domkyrka 1300-2000. Helsingfors.

Götze, J., 2012. Application of cathodoluminescence microscopy and spectroscopy in geosciences. Microsc. Microanal. 18 (6), 1270–1284.

Heinemeier, J., Ringbom, Å., Lindroos, A., Sveinbjornsdottir, A.E., 2010. Successful AMS C-14 dating of non-hydraulic lime mortars from the medieval churches of the Aland islands, Finland. Radiocarbon 52 (1), 171–204.

Hodgins, G., Lindroos, A., Ringbom, Å., Heinemeier, J., Brock, F., 2011. 14C dating of Roman mortars - preliminary tests using diluted hydrochloric acid injected in batches. Commentationes Humanarum Litterarum 128, 209–213.

Holdridge, G., 2020. The geology of the northwest quarter of ancient jerash within its regional context. In: Lichtenberger, A., Raja, R., (Eds.), Environmental Studies, Remote Sensing, and Modelling: Final Publications from the Danish-German Jerash Northwest Quarter Project I: Brepols Publishers. p 45-61.

Jackson, C.E., Saeger, C.M., 1935. Use of the pipette method in the fineness test of molding sand. J. Res. Nat. Bur. Stand. 14 (1), 59. https://doi.org/10.6028/jres.014.034.

Kalaitzoglou, G., Lichtenberger, A., Raja, R., forthcoming 1. Preliminary Report of the Fifth Season of the Danish-German Jerash Northwest Quarter Project 2015. Annual of the Department of Antiquities of Jordan(60).
Kalaitzoglou, G., Lichtenberger, A., Raja, R., forthcoming 2. Preliminary Report of the Sixth Season of the Danish-German Jerash Northwest Quarter Project 2016. Annual of the Department of Antiquities of Jordan(61).
Labeyrie, J., Delibrias, G., 1964. Dating of old mortars by carbon-14 method. Nature 201 (492), 742.
Lichtenberger, A., 2003. Kulte und Kultur der Dekapolis. Untersuchungen zu numismatischen, archäologischen und epigraphischen Zeugnissen. Harrassowitz Verlag, Wiesbaden.
Lichtenberger, A., Raja, R., 2015. An architectural block with altar-iconography from the North-west Quarter of Jerash *. Levant 47 (1), 112–130.
Lichtenberger, A., Lindroos, A., Raja, R., Heinemeier, J., 2015. Radiocarbon analysis of mortar from Roman and Byzantine water management installations in the Northwest Quarter of Jerash, Jordan. J. Archaeological Sci.-Rep. 2, 114–127.
Lichtenberger, A., Raja, R., Eger, C., Kalaitzoglou, G., Sørensen, A., 2016. A newly excavated private house in Jerash. Reconsidering aspects of continuity and change in material culture from Late Antiquity to the early Islamic period. Antiquité Tardive 24, 317–359.
Lichtenberger, A., Raja, R., 2017. Mosaicists at work: The organisation of mosaic production in Early Islamic Jerash. Antiquity 91 (358), 998–1010.
Lichtenberger, A., Raja, R., et al., 2018. Middle Islamic Jerash (9th century - 15th century) Archaeology and History of an Ayyubid-Mamluk settlement. Brepols Publishers, Turnhout.
Lichtenberger, A., Raja, R., et al., 2019. Byzantine and Umayyad Jerash Reconsidered Transitions, Transformations, Continuities. Brepols Publishers, Turnhout.
Lichtenberger, A., Raja, R., 2019. Defining borders: the Umayyad-Abbasid transition and the earthquake of AD 749 in Jerash. In: Lichtenberger, A., Raja, R. (Eds.), Byzantine and Umayyad Jerash Reconsidered Transitions, Transformations, Continuities. Brepols Publishers, Turnhout, pp. 265–286.
Lichtenberger, A., Raja, R., et al., 2020. Hellenistic and Roman Gerasa: the archaeology and history of a Decapolis city. Brepols Publishers, Turnhout.
Lindroos, A., Heinemeier, J., Ringbom, Å., Brasken, M., Sveinbjornsdottir, A., 2007. Mortar dating using AMS C-14 and sequential dissolution: Examples from medieval, non-hydraulic lime mortars from the Åland Islands, SW Finland. Radiocarbon 49 (1), 47–67.
Lindroos, A., Ringbom, Å., Kaisti, R., Heinemeier, J., Hodgins, G., Brock, F., 2011a. The oldest parts of Turku cathedral. C-14 chronology of fire damaged mortars. In: Hansson, J., Ranta, H. (Eds.), Archaeology and history of churches in Baltic region. Symposium, JUNE 8-12, 2010, Visby, Sweden. Visby: iVisby Tryckeri AB. p 108-21.
Lindroos, A., Heinemeier, J., Ringbom, Å., Brock, F., Sonck-Koota, P., Pehkonen, P., Suksi, J., 2011b. Problems in radiocarbon dating of Roman pozzolana mortars. Commentationes Humanarum Litterarum, 214–30.
Lindroos, A., Ranta, H., Heinemeier, J., Lill, J.O., 2014. C-14 chronology of the oldest Scandinavian church in use. An AMS/PIXE study of lime lump carbonate in the mortar. Nuclear Instruments & Methods in Physics Research Section B-Beam Interactions with Materials and Atoms 331, 220–224.
Lindroos, A., Ringbom, Å., Heinemeier, J., Hodgins, G., Sonck-Koota, P., Sjöberg, P., Lancaster, L., Kaisti, R., Brock, F., Ranta, H., Caroselli, M., Lugli, S., 2018. Radiocarbon dating historical mortars: lime lumps and/or binder carbonate? Radiocarbon 60 (3), 875–899.
Marshall, D.J., 1988. Cathodoluminescence of geological materials. Geol. Mag. 128, 404–405.
Marzaioli, F., Nonni, S., Passariello, I., Capano, M., Ricci, P., Lubritto, C., De Cesare, N., Eramo, G., Castillo, J.A.Q., Terrasi, F., 2013. Accelerator mass spectrometry C-14 dating of lime mortars: Methodological aspects and field study applications at CIRCE (Italy). Nuclear Instruments & Methods in Physics Research Section B-Beam Interactions with Materials and Atoms 294, 246–251.
McHugh, M.L., 2013. The Chi-square test of independence. Biochemia Medica 23 (2), 143–149.
Nawrocka, D., Michniewicz, J., Pawlyta, J., Pazdur, A., 2005. Application of radiocarbon method for dating of lime mortars. Geochronometria 24, 109–115.
Nonni, S., Marzaioli, F., Secco, M., Passariello, I., Capano, M., Lubritto, C., Mignardi, S., Tonghini, C., Terrasi, F., 2013. 14C mortar dating: the case of the medieval Shayzar citadel, Syria. Radiocarbon 55 (2), 514–525.
Olsen, J., Tikhomirov, D., Grosen, C., Heinemeier, J., Klein, M., 2017. Radiocarbon analysis on the New AARAMS 1MV Tandetron. Radiocarbon 59 (3), 905–913.
Ortega, L.A., Zuluaga, M.C., Alonso-Olazabal, A., Murelaga, X., Insausti, M., Ibanez-Etxeberria, A., 2012. Historic lime-mortar C-14 dating of Santa Maria la real (Zarautz, Northern Spain): extraction of suitable grain size for reliable C-14 dating. Radiocarbon 54 (1), 23–36.
Philippsen, B., Olsen, J., 2020. Radiocarbon dating and bayesian modelling. In: Lichtenberger, A., Raja, R., (Eds.), Environmental Studies, Remote Sensing, and Modelling: Final Publications from the Danish-German Jerash Northwest Quarter Project I: Brepols Publishers. p 191-238.
Press, W.H., Teukolsky, S.A., Vetterling, W.T., Flannery, B.P., 1992. Numerical Recipes in C The Art of Scientific Computing. Cambridge University Press, Cambridge.
Raja, R., 2012. Urban Development and Regional Identity in the Eastern Roman Provinces, 50 BC–AD 250: Aphrodisias, Ephesos, Athens. MuseumTusculanum Press, Copenhagen, Gerasa.
Reimer, P.J., Austin, W.E.N., Bard, E., Bayliss, A., Blackwell, P.G., Bronk Ramsey, C., Butzin, M., Cheng, H., Edwards, R.L., Friedrich, M., Grootes, P.M., Guilderson, T.P., Hajdas, I., Heaton, T.J., Hogg, A.G., Hughen, K.A., Kromer, B., Manning, S.W., Muscheler, R., Palmer, J.G., Pearson, C., van der Plicht, J., Reimer, R.W., Richards, D.A., Scott, E.M., Southon, J.R., Turney, C.S.M., Wacker, L., Adolphi, F., Büntgen, U., Capano, M., Fahrni, S.M., Fogtmann-Schulz, A., Friedrich, R., Köhler, P., Kudsk, S., Miyake, F., Olsen, J., Reinig, F., Sakamoto, M., Sookdeo, A., Talamo, S., 2020. The IntCal20 Northern Hemisphere Radiocarbon Age Calibration Curve (0–55 cal kBP). Radiocarbon 62 (4), 725–757.
Ringbom, Å., Lindroos, A., Heinemeier, J., Sonck-Koota, P., 2014. 19 years of mortar dating: learning from experience. Radiocarbon 56 (2), 619–635.
Stuiver, M., Polach, H.A., 1977. Reporting of C-14 data - discussion. Radiocarbon 19 (3), 355–363.
Stuiver, M., Smith, C.S. (Eds.), 1965. Radiocarbon dating of ancient mortar and plaster. *Proceedings of the 6th international conference on radiocarbon and tritium dating*, Eds R. M. Chatters and E.A. Olson. Washington D.C., Clearinghouse for Fed. Sci. & Tech. Inf. Natural Bur. Standards, U.S. Dept, Commerce, pp. 338–343.
Thomsen, K.D., 2019. Urban Life in Jerash, Jordan. Aarhus University, Aarhus.
Toffolo, M.B., Ricci, G., Chapoulie, R., Caneve, L., Kaplan-Ashiri, I., 2020. Cathodoluminescence and laser-induced fluorescence of calcium carbonate: a review of screening methods for radiocarbon dating of ancient lime mortars. Radiocarbon 62 (3), 545–564.
Van Strydonck, M., Dupas, M., Dauchotdehon, M., Pachiaudi, C., Marechal, J., 1986. The influence of contaminating (fossil) carbonate and the variations of delta-C-13 in mortar dating. Radiocarbon 28 (2A), 702–710.
Van Strydonck, M.J.Y., Dupas, M., Keppens, E., 1989. Isotopic fractionation of oxygen and carbon in lime mortar under natural environmental-conditions. Radiocarbon 31 (03), 610–618.
Van Strydonck, M.J.Y., Van Der Borg, K., de Jong, A.F.M., Keppens, E., 1992. Radiocarbon dating of lime fractions and organic material from buildings. Radiocarbon 34 (3), 873–879.
Vitruvius, M.M.H., 1914a. Book II, Chapter VIII, Methods of building walls. The ten books on architecture. Harvad University Press, Cambridge.
Vitruvius, M.M.H., 1914b. Book VII, Chapter I, Floors. The ten books on architecture. Harvad University Press, Cambridge.
Vogel, J.S., Southon, J.R., Nelson, D.E., Brown, T.A., 1984. Performance of catalytically condensed carbon for use in accelerator mass-spectrometry. Nuclear Instruments & Methods in Physics Research Section B-Beam Interactions with Materials and Atoms 5 (2), 289–293.
Wootton, W.T., 2017. Mosaics from the North-West Quarter of Jerash. In: Lichtenberger A, Raja R, editors. Gerasa/Jerash: from the Urban Periphery. Aarhus. p 89-98.
WTW, 2017. SenTix® 950 / 980 / Micro 900(-P). Weilheim, Germany: Xylem Analytics Germany.
Yaseen, I.A.B., Al-Amoush, H., Al-Farajat, M., Mayyas, A., 2013. Petrography and mineralogy of Roman mortars from buildings of the ancient city of Jerash, Jordan. Construction and Building Materials 38:465 - 71.